

MCNP6 fragmentation of light nuclei at intermediate energies

Stepan G. Mashnik^a, Leslie M. Kerby^{a,b}

In memory of Dick Prael, outstanding scientist and person

^aLos Alamos National Laboratory, Los Alamos, NM 87545, USA

^bUniversity of Idaho, Moscow, ID 83844, USA

Abstract

Fragmentation reactions induced on light target nuclei by protons and light nuclei of energies around 1 GeV/nucleon and below are studied with the latest Los Alamos Monte Carlo transport code MCNP6 and with its cascade-exciton model (CEM) and Los Alamos version of the quark-gluon string model (LAQGSM) event generators, version 03.03, used as stand-alone codes. Such reactions are involved in different applications, like cosmic-ray-induced single event upsets (SEU's), radiation protection, and cancer therapy with proton and ion beams, among others; therefore, it is important that MCNP6 simulates them as well as possible. CEM and LAQGSM assume that intermediate-energy fragmentation reactions on light nuclei occur generally in two stages. The first stage is the intranuclear cascade (INC), followed by the second, Fermi breakup disintegration of light excited residual nuclei produced after INC. Both CEM and LAQGSM account also for coalescence of light fragments (complex particles) up to ⁴He from energetic nucleons emitted during INC. We investigate the validity and performance of MCNP6, CEM, and LAQGSM in simulating fragmentation reactions at intermediate energies and discuss possible ways of further improving these codes.

Keywords: Monte Carlo, transport codes, MCNP6, cascade-exciton model (CEM), Los Alamos version of the quark-gluon string model (LAQGSM), fragmentation, Fermi breakup, coalescence, fragment spectra, production cross-sections

1. Introduction

Fragmentation reactions induced by protons and light nuclei of energies around 1 GeV/nucleon and below on light target nuclei are involved in different applications, like cosmic-ray-induced single event upsets (SEU's), radiation protection, and cancer therapy with proton and ion beams, among others. It is impossible to measure all nuclear data needed for such applications; therefore, Monte Carlo transport codes are usually used to simulate impacts associated with fragmentation reactions. It is important that available transport codes simulate such reactions as well as possible. For this reason, during the past several years, efforts have been done to investigate the validity and performance of, and to improve where possible, nuclear reaction models simulating fragmentation of light nuclei in GEANT4 [1], SHIELD-HIT [2]–[4], and PHITS [5, 6].

The Los Alamos Monte Carlo transport code MCNP6 [7] uses the latest version of the cascade-exciton model (CEM) as incorporated in its event generator CEM03.03 [8, 9] to simulate fragmentation of light nuclei at intermediate energies for reactions induced by nucleons, pions, and photons, and the Los Alamos version of the quark-gluon string model (LAQGSM) as implemented in the code LAQGSM03.03 [9, 10] to simulate fragmentation reactions induced by nuclei and by particles at higher energies, up to about 1 TeV/nucleon.

In recent years, MCNP6, with its CEM and LAQGSM event generators, has been extensively validated and verified (V&V)

against a large variety of nuclear reactions on both thin and thick targets (see, e.g. Refs. [11–14] and references therein), but was never tested specifically on fragmentation of light nuclei at intermediate energies. To address this, we investigate the performance of MCNP6, CEM, and LAQGSM in simulating fragmentation reactions at intermediate energies and discuss possible ways of further improving these codes.

2. A Brief Survey of CEM and LAQGSM Physics

Details, examples of results, and useful references to different versions of CEM and LAQGSM may be found in a recent lecture [9].

The Cascade-Exciton Model (CEM) of nuclear reactions was proposed more than 30 years ago at the Laboratory of Theoretical Physics, JINR, Dubna, USSR by Gudima, Mashnik, and Toneev [15]. It is based on the standard (non time-dependent) Dubna IntraNuclear Cascade (INC) [16, 17] and the Modified Exciton Model (MEM) [18, 19]. The code LAQGSM03.03 is the latest modification [10] of LAQGSM [20], which in its turn is an improvement of the Quark-Gluon String Model (QGSM) [21]. It describes reactions induced by both particles and nuclei at incident energies up to about 1 TeV/nucleon.

The basic version of both the CEM and LAQGSM event generators is the so-called “03.03” version, namely CEM03.03 [8, 9, 22] and LAQGSM03.03 [9, 10, 23]. The CEM code calculates nuclear reactions induced by nucleons, pions, and photons. It assumes that the reactions occur generally in three stages (see

Email address: mashnik@lanl.gov (Stepan G. Mashnik)

Fig. 1). The first stage is the INC, in which primary particles can be re-scattered and produce secondary particles several times prior to absorption by, or escape from the nucleus. When the cascade stage of a reaction is completed, CEM uses the coalescence model to “create” high-energy d, t, ^3He , and ^4He by final-state interactions among emitted cascade nucleons outside of the target. The emission of the cascade particles determines the particle-hole configuration, Z , A , and the excitation energy that is the starting point for the second, preequilibrium stage of the reaction. The subsequent relaxation of the nuclear excitation is treated in terms of an improved version of the modified exciton model of preequilibrium decay followed by the equilibrium evaporation/fission stage.

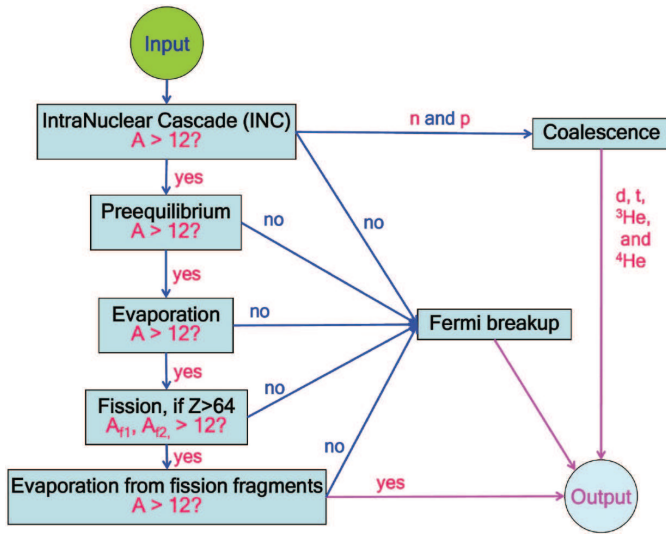


Figure 1: Flow chart of nuclear-reaction calculations by CEM03.03 and LAQGSM03.03.

Generally, all three components may contribute to experimentally measured particle spectra and other distributions. But if the residual nuclei after the INC have atomic numbers with $A \leq A_{Fermi} = 12$, CEM uses the Fermi breakup model to calculate their further disintegration instead of using the preequilibrium and evaporation models. Fermi breakup is much faster to calculate and gives results very similar to the continuation of the more detailed models to much lighter nuclei. LAQGSM also describes nuclear reactions, generally, as a three-stage process: INC, followed by preequilibrium emission of particles during the equilibration of the excited residual nuclei formed after the INC, followed by evaporation of particles from or fission of the compound nuclei. LAQGSM was developed with a primary focus on describing reactions induced by nuclei, as well as induced by most elementary particles, at high energies, up to about 1 TeV/nucleon. The INC of LAQGSM is completely different from the one in CEM. LAQGSM also considers Fermi breakup of nuclei with $A \leq 12$ produced after the cascade, and the coalescence model to “produce” high-energy d, t, ^3He , and ^4He from nucleons emitted during the INC.

Many people participated in the CEM and LAQGSM code development over their more than 40-year history. Current contributors to their “03.03” versions are S. G. Mashnik, K.

K. Gudima, A. J. Sierk, R. E. Prael, M. I. Baznat, and N. V. Mokhov. One of the authors (L.M.K.) has joined these efforts recently to extend the preequilibrium models of CEM and LAQGSM by accounting for possible emission of light fragment (LF) heavier than ^4He , up to ^{28}Mg .

2.1. The Intranuclear Cascade Mechanism

The INC approach is based on the ideas of Heisenberg and Serber, who regarded intranuclear cascades as a series of successive quasi-free collisions of the fast primary particle with the individual nucleons of the nucleus. Basic assumptions of and conditions for INC applicability may be found in [9]. Comprehensive details and useful references are published in [16, 17].

2.1.1. The INC of CEM03.03

The intranuclear cascade model in CEM03.03 is based on the standard (non-time-dependent) version of the Dubna cascade model [16, 17]. All the cascade calculations are carried out in a three-dimensional geometry. The nuclear matter density $\rho(r)$ is described by a Fermi distribution with two parameters taken from the analysis of electron-nucleus scattering. For simplicity, the target nucleus is divided by concentric spheres into seven zones in which the nuclear density is considered to be constant. The energy spectrum of the target nucleons is estimated in the perfect Fermi-gas approximation. The influence of intranuclear nucleons on the incoming projectile is taken into account by adding to its laboratory kinetic energy an effective real potential, as well as by considering the Pauli principle which forbids a number of intranuclear collisions and effectively increases the mean free path of cascade particles inside the target. The interaction of the incident particle with the nucleus is approximated as a series of successive quasi-free collisions of the fast cascade particles (N , π , or γ) with intranuclear nucleons.

The integral cross sections for the free NN , πN , and γN interactions are approximated in the Dubna INC model [16, 17] using a special algorithm of interpolation/extrapolation through a number of picked points, mapping as well as possible the experimental data. This was done very accurately by Prof. Barashenkov’s group using all experimental data available at that time, more than 45 years ago [24]. Currently the experimental data on cross sections is much more complete than at that time; therefore we have revised the approximations of all the integral elementary cross sections used in CEM.

The kinematics of two-body elementary interactions and absorption of photons and pions by a pair of nucleons is completely defined by a given direction of emission of one of the secondary particles. The cosine of the angle of emission of secondary particles in the c.m. system is calculated by the Dubna INC with approximations based on available experimental data. For elementary interactions with more than two particles in the final state, the Dubna INC uses the statistical model to simulate the angles and energies of products (see details in [16]).

For the improved version of the INC in CEM03.03, we use currently available experimental data and recently published systematics proposed by other authors and have developed new approximations for angular and energy distributions of particles

produced in nucleon-nucleon and photon-proton interactions. In addition, we have incorporated into newer versions of CEM a possibility to normalize the final results to systematics based on available experimental reaction cross sections. The condition for the transition from the INC stage of a reaction to preequilibrium was changed; on the whole, the INC stage in CEM03.03 is longer while the preequilibrium stage is shorter in comparison with previous versions. We have incorporated real binding energies for nucleons in the cascade instead of the approximation of a constant separation energy of 7 MeV used in the initial versions of the CEM and have imposed momentum-energy conservation for each simulated even (conservation was only “on the average” in earlier versions). Along with the improved elementary cross sections, we also changed and improved the algorithms of many INC routines and many INC routines were rewritten, which significantly speeded up the code. Details, examples of results, and references to this portion of our work may be found in [9].

2.1.2. The INC of LAQGSM03.03

The INC of LAQGSM03.03 is described with a recently improved version [10, 23, 25] of the time-dependent intranuclear cascade model developed initially at JINR in Dubna, often referred to in the literature as the Dubna intranuclear Cascade Model, DCM (see [26] and references therein). The DCM models interactions of fast cascade particles (“participants”) with nucleon spectators of both the target and projectile nuclei and includes as well interactions of two participants (cascade particles). It uses experimental cross sections at energies below 4.5 GeV/nucleon, and those calculated by the Quark-Gluon String Model [21, 27] at higher energies to simulate angular and energy distributions of cascade particles, and also considers the Pauli Exclusion Principle.

In contrast to the CEM version of the INC described above, DCM uses a continuous nuclear density distribution; therefore, it does not need to consider refraction and reflection of cascade particles inside or on the border of a nucleus. It also keeps track of the time of an intranuclear collision and of the depletion of the nuclear density during the development of the cascade (the so-called “trawling effect”) and takes into account the hadron formation time.

All the new approximations developed recently for the INC of CEM to describe total cross sections and elementary energy and angular distributions of secondary particles from hadron-hadron interactions have been incorporated also into the INC of LAQGSM [23]. In addition, a new high-energy photonuclear reaction model based on the event generators for γp and γn reactions from the Moscow INC [28] (kindly provided to us by Dr. Igor Pshenichnov) and on the latest photonuclear version of CEM [29] was developed and incorporated into the INC of LAQGSM; this allows us to calculate reactions induced by photons with energies of up to tens of GeV. In the latest version of LAQGSM [10], the INC was modified for a better description of nuclear reactions at very high energies (above 20 GeV/nucleon). Finally, the algorithms of many LAQGSM INC routines were revised and some INC routines were rewritten, which speeded up the code significantly. Details, examples of

results, and references to this portion of our work may be found in [9].

2.2. The Coalescence Model

When the cascade stage of a reaction is completed, CEM and LAQGSM use the coalescence model described in Ref. [26] to “create” high-energy d, t, ^3He , and ^4He by final-state interactions among emitted cascade nucleons outside of the target nucleus. In contrast to most other coalescence models for heavy-ion-induced reactions, where complex-particle spectra are estimated simply by convolving the measured or calculated inclusive spectra of nucleons with corresponding fitted coefficients, CEM03.03 and LAQGSM03.03 use in their simulations of particle coalescence real information about all emitted cascade nucleons and do not use integrated spectra. We assume that all the cascade nucleons having differences in their momenta smaller than p_c and the correct isotopic content form an appropriate composite particle. The coalescence radii p_c were fitted for each composite particle in Ref. [26] to describe available data for the reaction Ne+U at 1.04 GeV/nucleon, but the fitted values turned out to be quite universal and were subsequently found to describe high-energy complex-particle production satisfactorily for a variety of reactions induced both by particles and nuclei at incident energies up to about 200 GeV/nucleon, when describing nuclear reactions with different versions of LAQGSM [9] or with its predecessor, the Quark-Gluon String Model (QGSM) [21]. These parameters are:

$$\begin{aligned} p_c(d) &= 90 \text{ MeV}/c ; \\ p_c(t) &= p_c(^3\text{He}) = 108 \text{ MeV}/c ; \\ p_c(^4\text{He}) &= 115 \text{ MeV}/c . \end{aligned} \quad (1)$$

As the INC of CEM is different from those of LAQGSM or QGSM, it is natural to expect different best values for p_c as well. Our recent studies show that the values of parameters p_c defined by Eq. (1) are also good for CEM for projectile particles with kinetic energies T_0 lower than 300 MeV and equal to or above 1 GeV. For incident energies in the interval $300 \text{ MeV} \leq T_0 < 1 \text{ GeV}$, a better overall agreement with the available experimental data is obtained by using values of p_c equal to 150, 175, and 175 MeV/c for d, t (^3He), and ^4He , respectively. These values of p_c are fixed as defaults in CEM03.03. If several cascade nucleons are chosen to coalesce into composite particles, they are removed from the distributions of nucleons and do not contribute further to such nucleon characteristics as spectra, multiplicities, etc.

In comparison with the initial version [26], in CEM03.03 and LAQGSM03.03, several coalescence routines have been changed/deleted and have been tested against a large variety of measured data on nucleon- and nucleus-induced reactions at different incident energies.

2.3. Preequilibrium Reactions

The subsequent preequilibrium interaction stage of nuclear reactions is considered by our current CEM and LAQGSM in the framework of the latest version of the Modified Exciton

Model (MEM) [18, 19] as described in Ref. [22]. At the preequilibrium stage of a reaction, we take into account all possible nuclear transitions changing the number of excitons n with $\Delta = +2, -2$, and 0, as well as all possible multiple subsequent emissions of n, p, d, t, ^3He , and ^4He . The corresponding system of master equations describing the behavior of a nucleus at the preequilibrium stage is solved by the Monte-Carlo technique [15].

CEM considers the possibility of fast d, t, ^3He , and ^4He emission at the preequilibrium stage of a reaction in addition to the emission of nucleons. We assume that in the course of a reaction p_j excited nucleons (excitons) are able to condense with probability γ_j forming a complex particle which can be emitted during the preequilibrium state. The “condensation” probability γ_j is estimated as the overlap integral of the wave function of independent nucleons with that of the complex particle (see details in [15])

$$\gamma_j \approx p_j^3 (V_j/V)^{p_j-1} = p_j^3 (p_j/A)^{p_j-1}. \quad (2)$$

This is a rather crude estimate. As is frequently done, the values γ_j are taken from fitting the theoretical preequilibrium spectra to the experimental ones. In CEM, to improve the description of preequilibrium complex-particle emission, we estimate γ_j by multiplying the estimate provided by Eq. (2) by an empirical coefficient $M_j(A, Z, T_0)$ whose values are fitted to available nucleon-induced experimental complex-particle spectra.

CEM and LAQGSM predict forward-peaked (in the laboratory system) angular distributions for preequilibrium particles. For instance, CEM assumes that a nuclear state with a given excitation energy E^* should be specified not only by the exciton number n but also by the momentum direction Ω . This calculation scheme is easily realized by the Monte-Carlo technique [15]. It provides a good description of double differential spectra of preequilibrium nucleons and a not-so-good but still satisfactory description of complex-particle spectra from different types of nuclear reactions at incident energies from tens of MeV to several GeV. For incident energies below about 200 MeV, Kalbach [30] has developed a phenomenological systematics for preequilibrium-particle angular distributions by fitting available measured spectra of nucleons and complex particles. As the Kalbach systematics are based on measured spectra, they describe very well the double-differential spectra of preequilibrium particles and generally provide a better agreement of calculated preequilibrium complex-particle spectra with data than does the CEM approach [15]. This is why we have incorporated into CEM03.03 and LAQGSM03.03 the Kalbach systematics [30] to describe angular distributions of both preequilibrium nucleons and complex particles at incident energies up to 210 MeV. At higher energies, we use the CEM approach [15].

The standard version of the CEM [15] provides an overestimation of preequilibrium particle emission from different reactions we have analyzed (see more details in [31]). One way to solve this problem, suggested in Ref. [31], is to change the criterion for the transition from the cascade stage to the preequilibrium one. Another easy way, suggested in Ref. [31],

to shorten the preequilibrium stage of a reaction is to arbitrarily allow only transitions that increase the number of excitons, $\Delta n = +2$, *i.e.*, only allow the evolution of a nucleus toward the compound nucleus. In this case, the time of the equilibration will be shorter and fewer preequilibrium particles will be emitted, leaving more excitation energy for the evaporation. This approach was used in the CEM2k [31] version of the CEM and it allowed us to describe much better the p+A reactions measured at GSI in inverse kinematics at energies around 1 GeV/nucleon. Nevertheless, the “never-come-back” approach seems unphysical; therefore we no longer use it. We now address the problem of emitting fewer preequilibrium particles in the CEM by following Veselsky [32]. We assume that the ratio of the number of quasi-particles (excitons) n at each preequilibrium reaction stage to the number of excitons in the equilibrium configuration n_{eq} , corresponding to the same excitation energy, to be a crucial parameter for determining the probability of preequilibrium emission P_{pre} (see details in [9, 22, 32]). Algorithms of many preequilibrium routines were changed and almost all these routines were rewritten, which has speeded up the code significantly relative to earlier versions [9, 22].

2.4. Evaporation

CEM and LAQGSM use an extension of the Generalized Evaporation Model (GEM) code GEM2 by Furihata [33] after the preequilibrium stage of reactions to describe evaporation of nucleons, complex particles, and light fragments heavier than ^4He (up to ^{28}Mg) from excited compound nuclei and to describe fission, if the compound nuclei are heavy enough to fission ($Z \geq 65$).

When including evaporation of up to 66 types of particles in GEM2, running times increase significantly compared to the case when evaporating only 6 types of particles, up to ^4He . The major particles emitted from an excited nucleus are n, p, d, t, ^3He , and ^4He . For most cases, the total emission probability of particles heavier than α is negligible compared to those for the emission of light ejectiles. Our detailed investigation of different reactions shows that if we study only nucleon and complex-particle spectra or only spallation and fission products and are not interested in light fragments, we can consider evaporation of only 6 types of particles in GEM2 and save much time, getting results very close to the ones calculated with the more time consuming “66” option. In our current code versions, we allow the number of types of evaporated particles to be selected in advance. A detailed description of GEM2, as incorporated into CEM and LAQGSM, may be found in [9, 22].

2.5. Fission

The fission model used in GEM2 is based on Atchison’s model [34], often referred in the literature as the Rutherford Appleton Laboratory (RAL) fission model, which is where Atchison developed it. The mass-, charge-, and kinetic energy-distribution of fission fragments are simulated by RAL using approximations based on available experimental data (see details in [9, 22, 33, 34]). For CEM03.03 and LAQGSM03.03, we modified slightly [35] GEM2. Since in this study we consider only reactions on light, not fissioning nuclei, we will not

discuss further the fission model; interested readers may find details and further references in [9, 22, 35, 36].

2.6. The Fermi Breakup Model

After calculating the coalescence stage of a reaction, CEM and LAQGSM move to the description of the last slow stages of the interaction, namely to preequilibrium decay and evaporation, with a possible competition of fission. But at any stage, if the residual nuclei have atomic numbers with $A \leq A_{Fermi} = 12$, CEM and LAQGSM use the Fermi breakup model [37] to calculate their further disintegration instead of using the preequilibrium and evaporation models. All formulas and details of the algorithms used in the version of the Fermi breakup model developed in the group of the Late Prof. Barashenkov at JINR, Dubna, may be found in [38]; we use this model.

The original version of the model contained a few features which very occasionally could lead to unphysical fragments; these could cause problems in a transport model. All these issues have been dealt with in the current version, which no longer encounters such problems.

3. Results

As described above, de-excitation of light nuclei with $A \leq A_{Fermi}$ produced after the INC is described by CEM and LAQGSM only with the Fermi break-up model, where A_{Fermi} is a “cut-off value” fixed in our models. The value of A_{Fermi} is a model dependent parameter, not a physics characteristic of nuclear reactions. Actually, the initial version of the Fermi breakup model we incorporated in CEM and LAQGSM [22, 23] was used when $A \leq A_{Fermi} = 16$, just as $A_{Fermi} = 16$ is used currently in GEANT4 (see [1]) and in SHIELD-HIT (see [2]–[4]). But as mentioned in Section 2.6, that initial version of the Fermi breakup model had some problems and crashed our codes in some cases. To avoid unphysical results and code crashes, we chose the expedient of using $A_{Fermi} = 12$ in both CEM and LAQGSM. Later, we fixed the problems in the Fermi break-up model, but did not at that time change the value of A_{Fermi} , and never studied how its value affects the final results calculated in these codes. We address this here, calculating spectra of emitted particles and light fragments, and yields of all possible products from various reactions using different values for A_{Fermi} . We discuss below separately product cross sections (Section 3.1) and spectra of particles and light fragments (Section 3.2).

3.1. Fragment production cross sections

One of the most difficult tasks for any theoretical model is to predict cross sections of arbitrary products as functions of the incident energy of the projectiles initiating the reactions, *i.e.*, excitation functions. Therefore, we chose to start our study with comparing the available experimental data on excitation functions of products from several proton-induced reactions on light nuclei at intermediate energies with predictions by MCNP6 using its default event generator for such reactions, CEM03.03, as well as with results calculated by CEM03.03 used as a stand-alone code.

Figs. 2–15 present examples of excitation functions for all products we found at least several measured values for proton-induced reactions on ^{14}N , ^{16}O , ^{27}Al , and ^{28}Si . To understand better the reasons of agreements or disagreements of calculated values with the measured excitation functions, we present in our figures also the total reaction cross sections, experimental and theoretical.

Figs. 2–5 show our results for the $p + ^{14}\text{N}$ reaction. The first thing to note is that the total reaction cross sections simulated with MCNP6 and shown in the upper-left plot in Fig. 2 with small solid circles agree well with the available experimental data (symbols) and with calculations by CEM03.03 used as a stand-alone code (solid line). There is a difference between the models, especially in the regions of incident proton energies $T_p = 50 - 100$ MeV and $T_p \geq 2$ GeV. To be expected, since MCNP6 and CEM03.03 use very similar, but slightly different approximations for the total proton-nucleus reaction cross sections (see details and references in [7, 8]). These little differences in the total reaction cross sections will produce, respectively, similar differences in all excitation functions simulated with MCNP6 and CEM03.03.

The total reaction cross sections are based on systematics (see details and references in [7, 8]), therefore they do not depend on the value of A_{Fermi} we use in our calculations. However, we performed calculations of all excitation functions shown in Figs. 2 to 5 with CEM03.03 used as a stand-alone code with its “default value” $A_{Fermi} = 12$, as well as with a modification of the code using $A_{Fermi} = 16$, which in case of these $p + ^{14}\text{N}$ reactions, actually corresponds to $A_{Fermi} = 14$. We cannot get a mass number $A = 16$ from $p + ^{14}\text{N}$ interactions, and even a nucleus with $A = 15$ would not be produced by the INC of CEM03.03 at these intermediate energies.

First, from the results presented in Figs. 2 to 5, we see a very good agreement between the excitation functions simulated by MCNP6 using CEM03.03 and calculations by CEM03.03 used as a stand-alone code, and a reasonable agreement with most of available experimental data. This fact serves as a validation and verification (V&V) of MCNP6 and shows no problems with the implementation of CEM03.03 in MCNP6 or with the simulations of these reactions by either code.

Second, we’d like to explicitly inform the readers that we do not worry too much about some observed discrepancies between some calculated excitation functions and measured data at low energies, below 20 MeV. As the default, MCNP6 uses data libraries at such low energies and never uses CEM03.03 or its other event generators, if data libraries are available (MCNP6 has proton-induced data libraries for the reactions studied here). By contrast, CEM uses its INC to simulate the first stage of nuclear reactions, and the INC is not supposed to work properly at such low energies (see details in [8, 9]).

Third, results calculated both with $A_{Fermi} = 12$ and 16 agree reasonably well with available data, taking into account that all calculations, at all energies and for all reactions were done with the fixed version of our codes, without any tuning or changing of any parameters. However, in some cases, we can observe significant differences between excitation functions calculated with $A_{Fermi} = 12$ and 16.

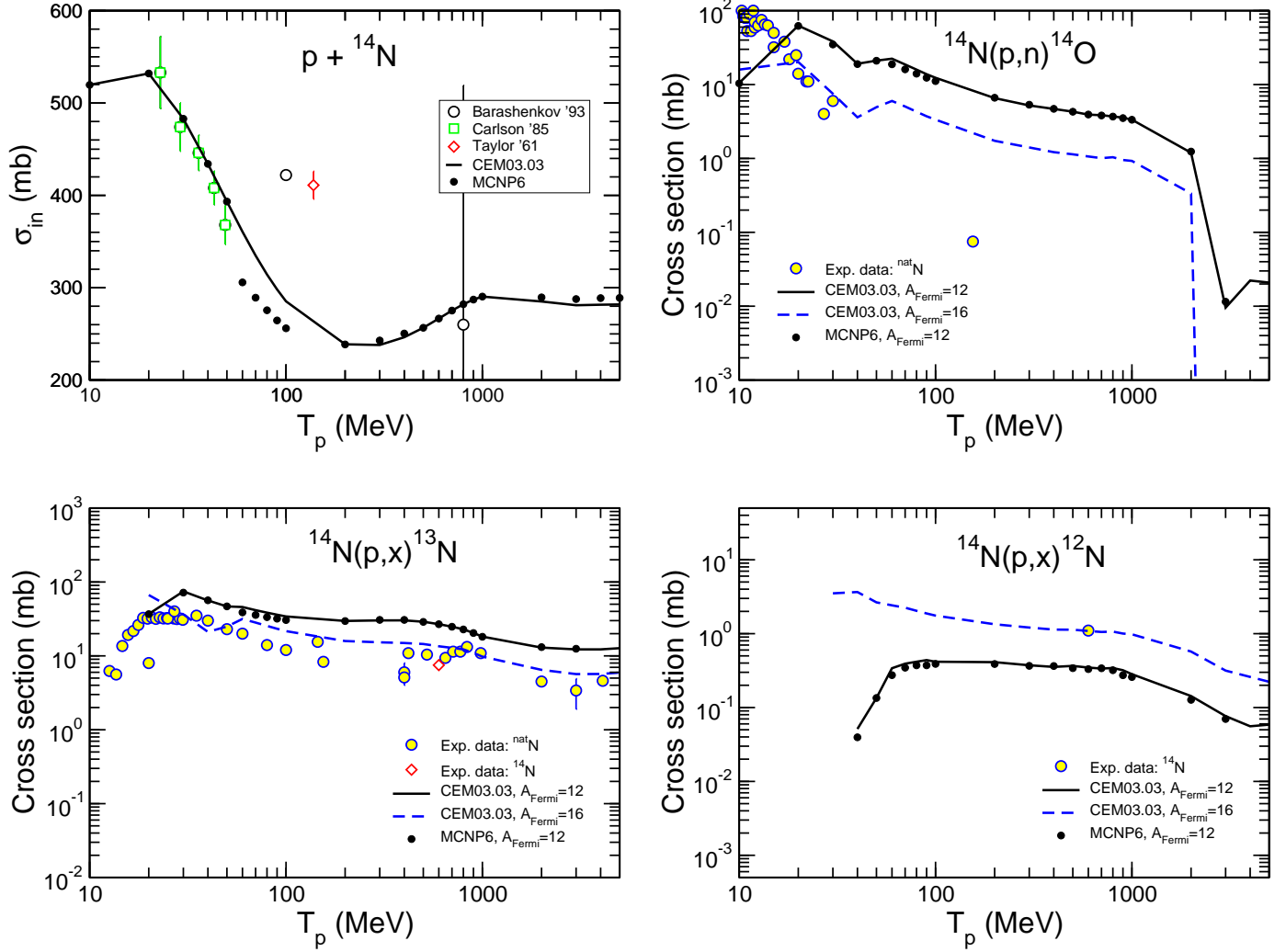


Figure 2: Total inelastic cross section and excitation functions for the production of ^{14}O , ^{13}N , and ^{12}N from $p + ^{14}\text{N}$ calculated with CEM03.03 using the “standard” version of the Fermi breakup model ($A_{\text{Fermi}} = 12$) and with a cut-off value of 16 for A_{Fermi} , as well as with MCNP6 using CEM03.03 ($A_{\text{Fermi}} = 12$) compared with experimental data, as indicated. Experimental data for inelastic cross sections are from Refs. [39]–[41], while the data for excitation functions are from the T16 Lib compilation [42].

For this particular reaction, the excitation functions for the production of ^{14}O , ^{13}N , ^{12}N , ^{13}C , ^{12}C , and ^{10}C calculated with $A_{\text{Fermi}} = 16$ (that for our $p + ^{14}\text{N}$ reaction is the same as $A_{\text{Fermi}} = 14$, which from a physical point of view means that we use only Fermi breakup after INC and never use preequilibrium and/or evaporation models to calculate this reaction) agree better with available experimental data than results obtained with $A_{\text{Fermi}} = 12$. On the other hand, excitation functions for the production of ^9Be and ^7Be are reproduced better with $A_{\text{Fermi}} = 12$.

Figs. 6 to 9 present results similar to the ones shown in Figs. 2 to 5, but for the reaction $p + ^{16}\text{O}$. Most of the experimental data for these reactions were measured on ^{nat}O , with only a few data points obtained for ^{16}O ; all our calculations were performed for ^{16}O . For these reactions, we performed three sets of calculations, using $A_{\text{Fermi}} = 12, 14,$ and 16 in CEM03.03. The general agreement/disagreement of our results with available measured data for oxygen is very similar to what we showed above for $p + ^{14}\text{N}$, with the major difference that almost all

products from oxygen are better predicted with $A_{\text{Fermi}} = 14$; production of ^{11}B is described a little better with $A_{\text{Fermi}} = 16$, while ^9Be and ^7Be are reproduced better with $A_{\text{Fermi}} = 12$, just as for nitrogen (see Figs. 4 and 5).

Figs. 10 to 15 show results similar to those in Figs. 2–9, but for proton interactions with ^{27}Al and ^{28}Si . All reactions on silicon were calculated for ^{28}Si , while most of the data were measured from ^{nat}Si (see details in legends of Fig. 14). Aluminum and silicon are interesting because they are used in many applications. From a theoretical point of view, $p + ^{27}\text{Al}$ and ^{28}Si reactions are challenging because Al and Si are relatively light, with significant contributions from the Fermi breakup models in our simulations. At the same time Al and Si have mass numbers higher than the discussed above, allowing some significant contribution to the calculated values from preequilibrium and evaporation processes. On the whole, the agreement of the results with available measured data for Al and Si is very similar to what we find for N and O. In many cases, we get a better

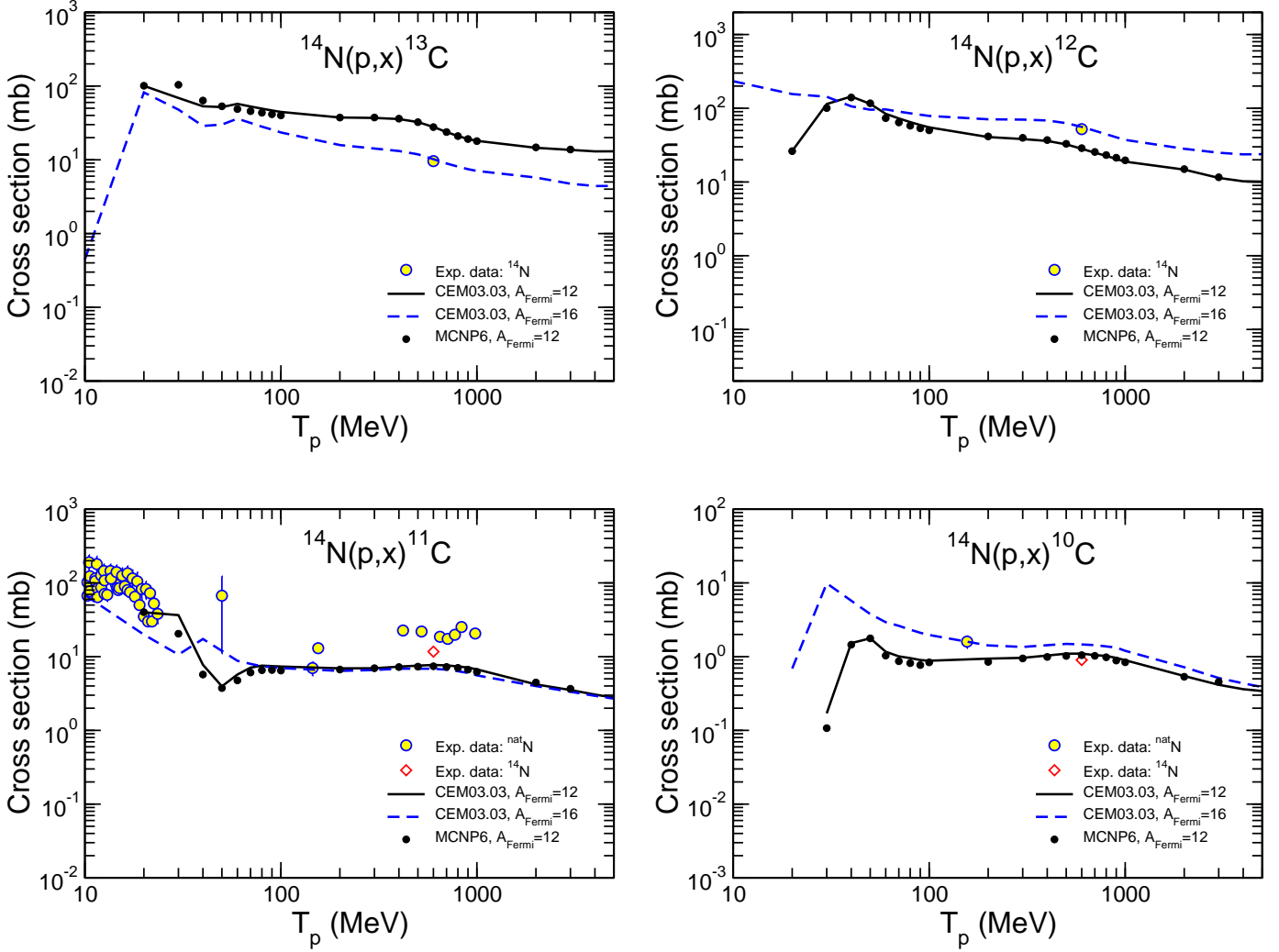


Figure 3: Excitation functions for the production of ^{13}C , ^{12}C , ^{11}C , and ^{10}C from $p + ^{14}\text{N}$ calculated with CEM03.03 using the “standard” version of the Fermi breakup model ($A_{\text{Fermi}} = 12$) and with a cut-off value of 16 for A_{Fermi} , as well as with MCNP6 using CEM03.03 ($A_{\text{Fermi}} = 12$) compared with experimental data, as indicated. Experimental data are from the T16 Lib compilation [42].

description of the heavy fragments when we use $A_{\text{Fermi}} = 16$ or 14, and usually we predict a little better the light fragments using $A_{\text{Fermi}} = 12$. For comparison, for Al and Si, we show also excitation functions for the production of all complex particles from d to ^4He , as well as of secondary protons, as we found experimental data available for them. Because the absolute values of the yields of light fragment production is much lower compared to the yields of complex particles, and especially of protons, the production cross sections of d, t, ^3He , ^4He , and especially of p calculated with different values of A_{Fermi} are very close to each other. This is true also for the production of neutrons; although we do not have experimental data for neutron production for these reactions. Generally, emission of nucleons and complex particles are the most determinative in the calculation of spallation products (heavier residuals) from reactions on medium-mass nuclei, while LF yields are generally low, and their calculation does not affect significantly the final cross sections for these heavier products.

Figs. 16 and 17 show mass-number dependences of the yield

of H, He, Li, Be, B, C, N, and O isotopes produced in 600 MeV $p + ^{16}\text{O}$, with a comparison of our CEM results calculated with $A_{\text{Fermi}} = 12$ and 16 with measured data from Ref. [47]. There is a relatively good agreement of both values of A_{Fermi} , which does not allow us to choose a preferred value. The yields of ^{11}B , ^{12}B , and ^{14}O with $A_{\text{Fermi}} = 16$ agree better with the data, while that of ^{12}N is predicted better using $A_{\text{Fermi}} = 12$.

Fig. 18 shows an example of one more type of nuclear reaction characteristic: Atomic-number dependence of the fragment-production cross sections from the interactions of ^{20}Ne (600 MeV/nucleon) with H. For this reaction, besides experimental data from Ref. [49], we compare to results calculated with CEM03.03 used as a stand-alone code with $A_{\text{Fermi}} = 12$ and 16, results by MCNP6 using the CEM03.03 event generator with $A_{\text{Fermi}} = 12$, as well as results by the NASA semi-empirical nuclear fragmentation code NUCFRG2 [50], and by a parameterization by Nilsen et al. [51] taken from Tab. III of Ref. [49]. We see that all models agree quite well with the measured data, especially for LF with $Z > 4$. For

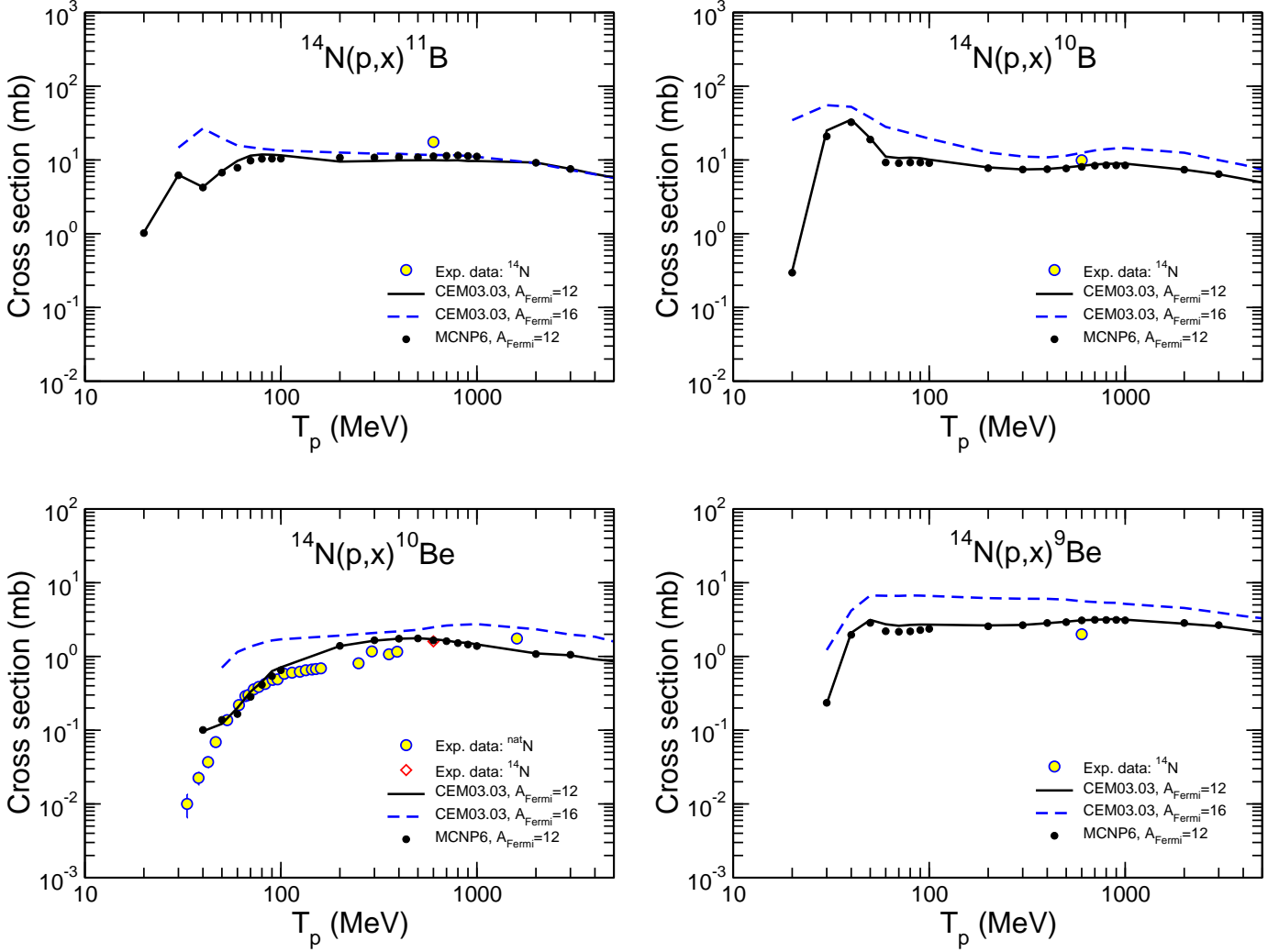


Figure 4: The same as in Fig. 3, but for the production of ^{11}B , ^{10}B , ^{10}Be , and ^9Be .

LF with $Z > 4$, it is difficult to determine from which version of CEM03.03 results agree better with the data: the one using $A_{\text{Fermi}} = 12$ or the one with $A_{\text{Fermi}} = 16$. Light fragments with $Z = 3$ and 4 are described a little better with the $A_{\text{Fermi}} = 12$ version. As we discuss at the end of the next Section, pre-equilibrium emission described with an extended version of the MEM (not accounted for in our calculations shown in Fig. 18), can be important and may change the final CEM results for this reaction; therefore we are not ready to make a final decision about which version of the Fermi breakup model works better for this system.

All the examples in Figs. 2 to 18 are for reactions induced by protons, which at such relatively low incident energies are simulated by default in MCNP6 with CEM03.03. Figs. 19 and 20 show examples of nucleus-nucleus reactions with light nuclei, *i.e.*, involving the Fermi breakup model, but simulated in MCNP6 with LAQGSM03.03. The figures compare experimental [48, 49] Z -dependences of products from interactions of 290 MeV/nucleon ^{14}Ne and ^{16}O with C and Al; 600 MeV/nucleon ^{20}Ne with C and Al; and 400 MeV/nucleon ^{24}Mg

with C and Al with LAQGSM03.03 results using $A_{\text{Fermi}} = 12$ and 16, as well as with results of calculations using models of Refs. [50, 51, 52], in the case of 600 MeV/nucleon $^{20}\text{Ne} + \text{C}$ and Al.

The cross sections shown in Figs. 19 and 20 are only for the fragmentation of the projectile-nuclei ^{14}N , ^{16}O , ^{20}Ne , and ^{24}Mg ; they do not contain contributions from the fragmentation of the C and Al target-nuclei. For all calculations using all models general agreement to the experimental data is quite good. On the whole, for these particular reactions, the products with $Z = 3$ and 4 are described a little better with the $A_{\text{Fermi}} = 12$ version of LAQGSM, while heavier fragments are often predicted better with $A_{\text{Fermi}} = 16$.

3.2. Fragment spectra

This Section presents several examples of particle and LF spectra from various proton- and nucleus-induced reactions, chosen so that although all of them are fragmentation of light nuclei at intermediate energies, they address different reaction mechanisms of fragment production, sometimes involving sev-

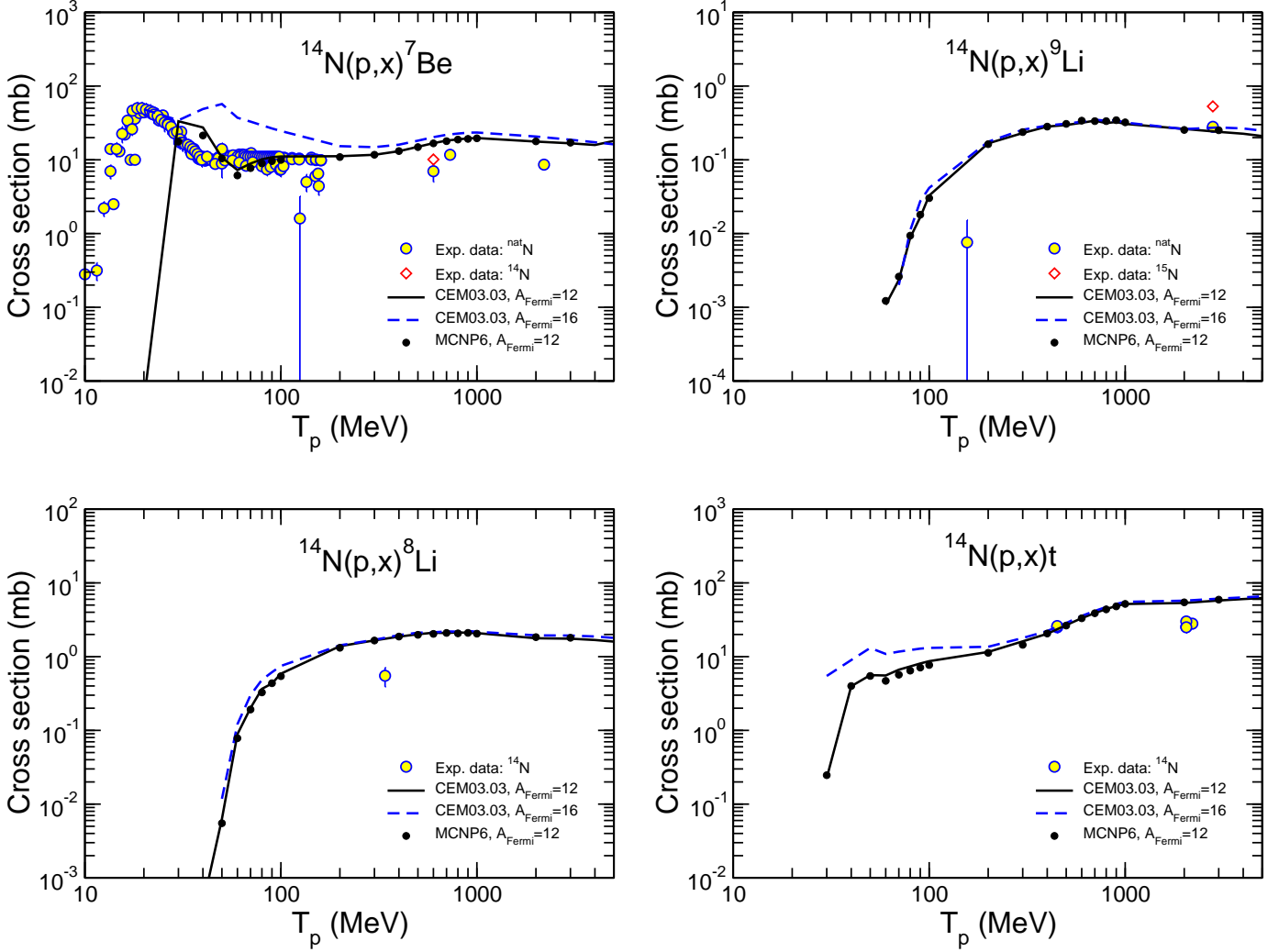


Figure 5: The same as in Fig. 3, but for the production of ${}^7\text{Be}$, ${}^9\text{Li}$, ${}^8\text{Li}$, and t .

eral mechanisms in the production of the same LF in a given reaction.

Figs. 21 to 23 show examples of measured particle and LF double-differential spectra from $p + {}^9\text{Be}$ at 190 and 300 MeV [53], as well as at 392 MeV [54] (symbols) compared with our CEM results (histograms). Because ${}^9\text{Be}$ has a mass number $A < A_{\text{Fermi}} = 12$, all the LF from these reactions are calculated by CEM either as fragments from the Fermi breakup of the excited nuclei remaining after the initial INC stage of reactions, or as “residual nuclei” after emission during INC of several particles from the ${}^9\text{Be}$ target nucleus. No preequilibrium or/and evaporation mechanisms are considered for these reactions by CEM. There is quite a good agreement of the CEM predictions with the measured spectra from ${}^9\text{Be}$ for all products shown in this example: protons (300 MeV $p + \text{Be}$), complex particles (t from 300 MeV $p + \text{Be}$ and ${}^3\text{He}$ and ${}^4\text{He}$ from 190 and 392 MeV $p + \text{Be}$), and heavier ${}^6\text{He}$ to ${}^7\text{Be}$.

Fig. 24 shows examples of similar LF spectra from a carbon nucleus, where only INC and Fermi breakup reaction mechanisms are considered by our CEM. CEM produces He and Li

from these reaction via Fermi breakup after INC, while Be and B are probably produced as residual nuclei after emitting several nucleons during INC from the carbon target nucleus. The general agreement of the CEM predictions with these measured LF spectra is quite good, taking into account that no fitting or changing of any parameters in CEM was done; we used the fixed version of CEM03.03 as implemented in MCNP6.

Fig. 25 shows similar examples of LF spectra, namely, double-differential spectra at 45 degrees of Li, Be, B, and C from ${}^{14}\text{N}$ and ${}^{16}\text{O}$ nuclei bombarded with 70 MeV protons. With these higher mass numbers, we performed calculations with CEM03.03 using also $A_{\text{Fermi}} = 14$ and 16, to see how different values affect the final LF spectra. The general agreement of our CEM results with these LF spectra is reasonably good, but not quite as good as seen in Figs. 21 to 24. On the whole, for these particular reactions, CEM03.03 provides a better agreement with the measured LF spectra with $A_{\text{Fermi}} = 12$.

The examples of LF spectra shown in Figs. 21–25 address fragmentation of light targets with proton beams. We present also several examples of LF spectra from nucleus-nucleus re-

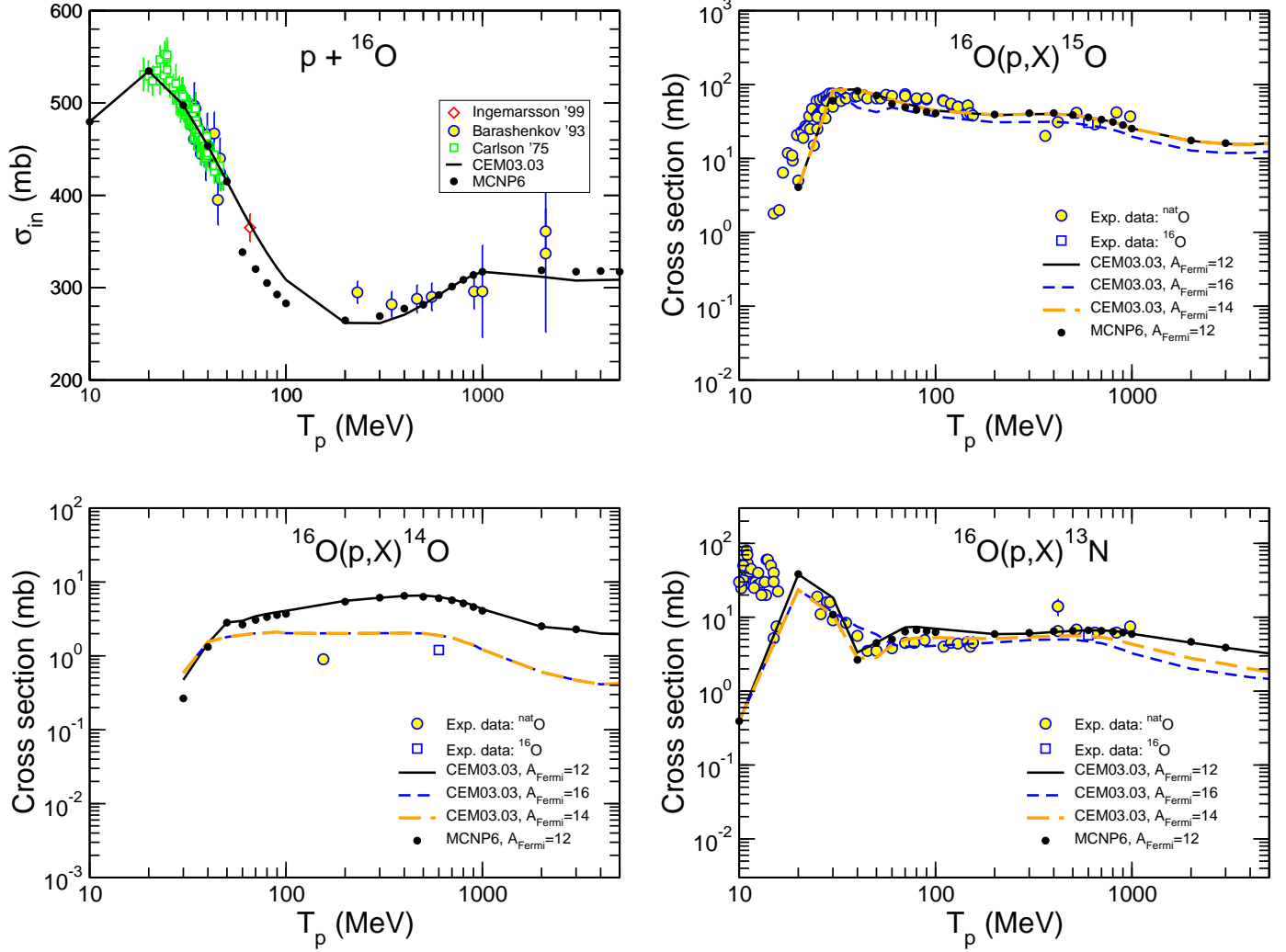


Figure 6: Total inelastic cross section and excitation functions for the production of ^{15}O , ^{14}O , and ^{13}N from $p + ^{16}\text{O}$ calculated with CEM03.03 using the “standard” version of the Fermi breakup model ($A_{\text{Fermi}} = 12$) and with cut-off values for A_{Fermi} of 16 and 14, as well as with MCNP6 using CEM03.03 ($A_{\text{Fermi}} = 12$) compared with experimental data, as indicated. Experimental data for inelastic cross sections are from Refs. [39, 43, 44], while the data for excitation functions are from the T16 Lib compilation [42].

actions. Actually, we have already tested MCNP6 against almost all available particle and LF data up to ^4He spectra from various nucleus-nucleus reactions at intermediate energies. As a rule, MCNP6 using its LAQGSM03.03 event generator describe such spectra quite well (see e.g., Refs. [11, 13, 14] and references therein). The cases where there is a good agreement with experimental data are valuable for MCNP6, to verify its predictive power, but are not so interesting for this study, as they do not address unsolved problems in the LAQGSM event-generator. One of the worst discrepancies of the LAQGSM LF spectra with available data found from this V&V of MCNP6 is shown below in Fig. 26 with dotted lines, namely calculated with the standard version of LAQGSM invariant spectra of p , d , t , and ^3He from 800 MeV/nucleon $^{20}\text{Ne} + ^{20}\text{Ne}$ compared with experimental data from Refs. [57, 58]. ^{20}Ne nuclei are light enough for the subject of our current work, but their mass number $A > A_{\text{Fermi}} = 12$, therefore LF can be produced by LAQGSM not only with the Fermi breakup model, when the

residual excited nucleus after INC has a mass number $A < 13$, but also via preequilibrium emission and evaporation, as well as final residual nuclei after all stages of reactions (see. Fig. 1).

Only LF of high and very high energies were measured in those experiments at Bevatron/Bevalac at the Lawrence Berkeley Laboratory [57, 58], and only products from the fragmentation of the bombarding nuclei were detected. LAQGSM can reproduce such high-energy portions of spectra only with its coalescence model, as the Fermi breakup model would provide LF of lower energies, while the preequilibrium emission and evaporation would provide much lower LF energies; the energies of the LF produced as final “residual nuclei” after all other stages of reactions would be even much lower. In other words, the experimental data from Refs. [57, 58] are very convenient to test the coalescence model in LAQGSM.

As noted in Section 2.2, LAQGSM uses fixed values for p_c as determined by Eq. (1). Results obtained with such “standard” values for p_c are shown in Fig. 26 with dotted lines: We see

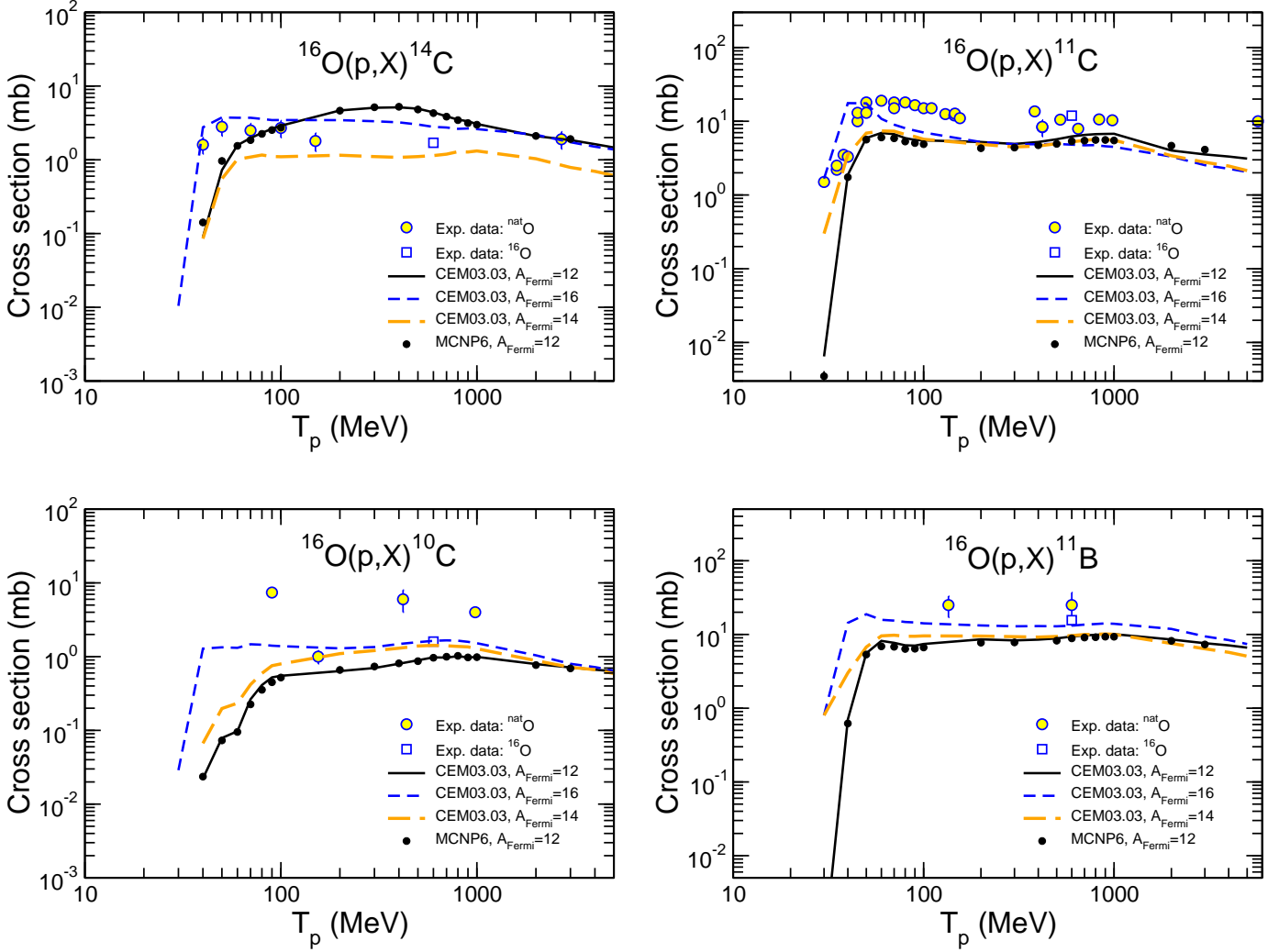


Figure 7: Excitation functions for the production of ^{14}C , ^{11}C , ^{10}C , and ^{11}B from $p + ^{16}\text{O}$ calculated with CEM03.03 using the “standard” version of the Fermi breakup model ($A_{\text{Fermi}} = 12$) and with cut-off values for A_{Fermi} of 16 and 14, as well as with MCNP6 using CEM03.03 ($A_{\text{Fermi}} = 12$) compared with experimental data, as indicated. Experimental data are from the T16 Lib compilation [42].

that these LAQGSM spectra underestimate the measured data, suggesting that we need to use higher values for p_c , at least for this particular reaction. As a second test of p_c values, we try to use for this reaction the values

$$\begin{aligned}
 p_c(d) &= 115 \text{ MeV}/c ; \\
 p_c(t) &= p_c(^3\text{He}) = \\
 &= p_c(^4\text{He}) = 175 \text{ MeV}/c ,
 \end{aligned}
 \tag{3}$$

found to work the best in CEM03.03 in the $300 \text{ MeV} \leq T < 1 \text{ GeV}$ region of incident energies. Results obtained with these values for p_c are shown in Fig. 26 with dashed lines: We see that values of p_c defined by Eq. (3) provide too many high energy LF, *i.e.*, these values are too big to provide the best results for LF spectra calculated by LAQGSM for this particular reaction. Finally, we try some intermediate p_c values:

$$\begin{aligned}
 p_c(d) &= 120 \text{ MeV}/c ; \\
 p_c(t) &= p_c(^3\text{He}) = \\
 &= p_c(^4\text{He}) = 140 \text{ MeV}/c .
 \end{aligned}
 \tag{4}$$

Results calculated with these values are shown with solid lines in Fig. 26: They agree much better with the measured spectra of d , t , and ^3He from this reaction than the previous two sets of results. Note that the aim of our work is not to fine-tune the parameters used by the coalescence model in our CEM and LAQGSM event generators. We may consider such a fine-tuning at a later stage, after we complete our work on extension of the preequilibrium model to account for possible emission of LF heavier than ^4He at the preequilibrium stage of reactions, discussed below. Here, we just show that although the standard versions of our CEM and LAQGSM event generators for MCNP6 provide an overall good agreement of calculated spectra and yields of products from various reactions, a fine-tuning of some of their parameters would allow improving further the agreement of calculated results with available experimental data.

Finally, we mention briefly our preliminary results from recent work [59, 60] to extend the CEM and LAQGSM for accounting possible emission of LF heavier than ^4He (up to ^{28}Mg)

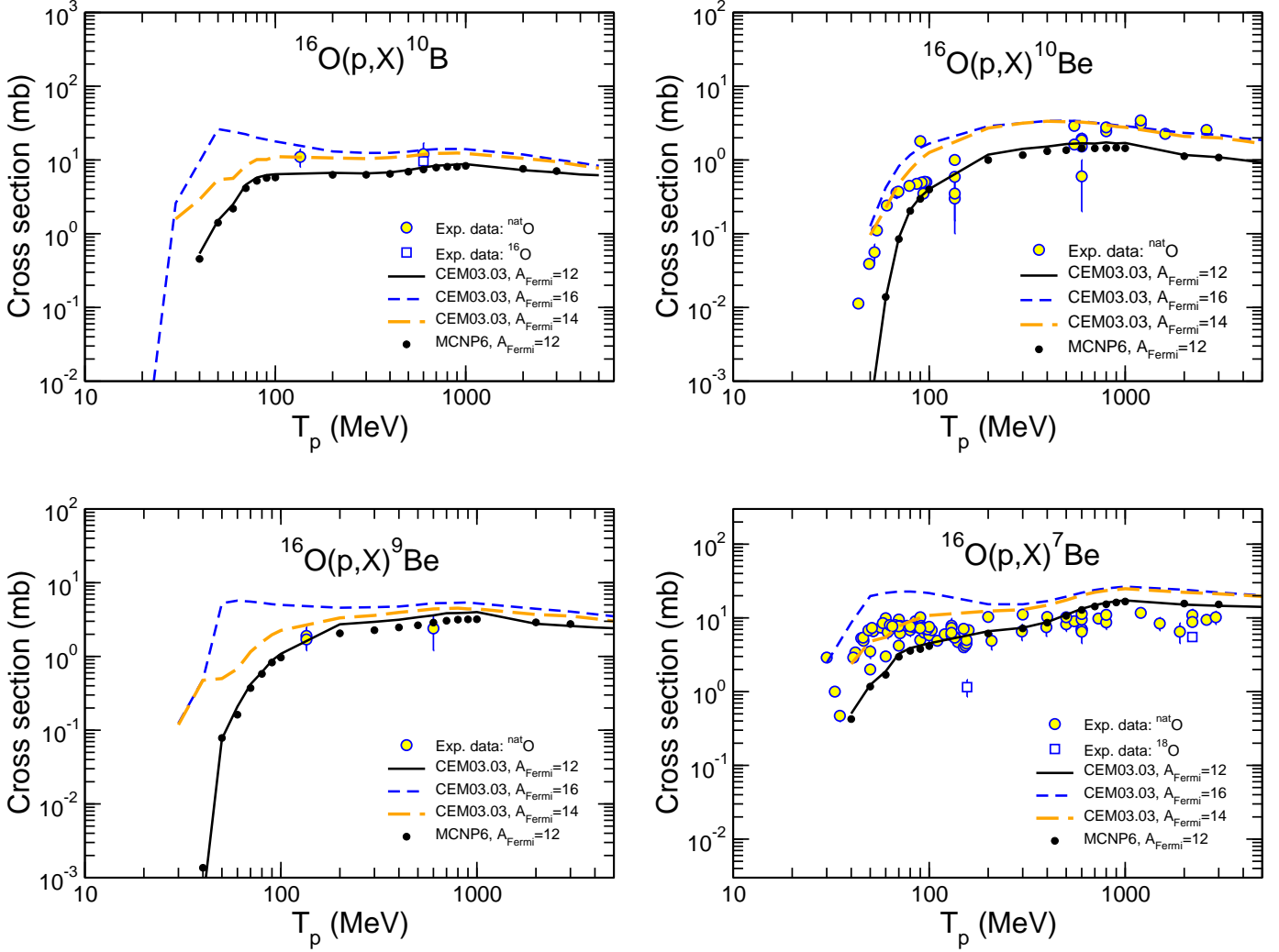


Figure 8: The same as in Fig. 7, but for the production of ^{10}B , ^{10}Be , ^9Be , and ^7Be .

at the preequilibrium stage of nuclear reactions. Fig. 27 shows an example of such results, namely, ^6Li spectra from the reaction $200\text{ MeV } p + ^{27}\text{Al}$ measured by Machner et al. [61] (symbols) compared with our preliminary results by an extended version of CEM, as described in Refs. [59, 60] (solid lines) and with results by the standard unmodified CEM (dashed lines). The aluminum target is relatively light, *i.e.*, such reactions are completely in the scope of this study. However, in comparison with lighter targets like C, N, and O discussed above, Al is heavier, the mass number of excited nuclei produced after INC from such reactions is mostly higher than 12, therefore CEM uses the preequilibrium and evaporation models to calculate this reaction, in addition to INC, coalescence, and Fermi breakup models (see Fig. 1).

The ^6Li spectra calculated with the standard version of CEM as implemented at present in MCNP6 shown with dashed histograms came mostly from evaporation of ^6Li from compound nuclei, and also contain a small contribution from Fermi breakup of excited nuclei with $A \leq A_{\text{Fermi}} = 12$ produced in a few cases after INC from Al-target, at such a relatively low

incident energy of only 200 MeV. As expected, evaporation of ^6Li from compound nuclei together with a small contribution from Fermi breakup of nuclei with $A \leq A_{\text{Fermi}} = 12$ produced after INC in this reaction do not provide enough high-energy LF emission, and the calculated ^6Li spectra do not extend to high energies and are below the measured data. Extension of the preequilibrium model used by CEM and LAQGSM to account for emission of LF heavier than ^4He as described in Refs. [59, 60], allows us to produce energetic LF from such reactions, improving the agreement with many measured LF spectra we tested so far. Of course, preequilibrium emission of LF is most important for medium and heavy target nuclei. But as we see in this example, it also affects significantly such relatively light nuclei as Al. Our work on extending the preequilibrium model in CEM and LAQGSM is incomplete. Results from this study will be published in the future. After completing this work, we may consider a fine-tuning of the A_{Fermi} parameter of the Fermi breakup model and of the coalescence model parameters used by the CEM and LAQGSM event generators of MCNP6.

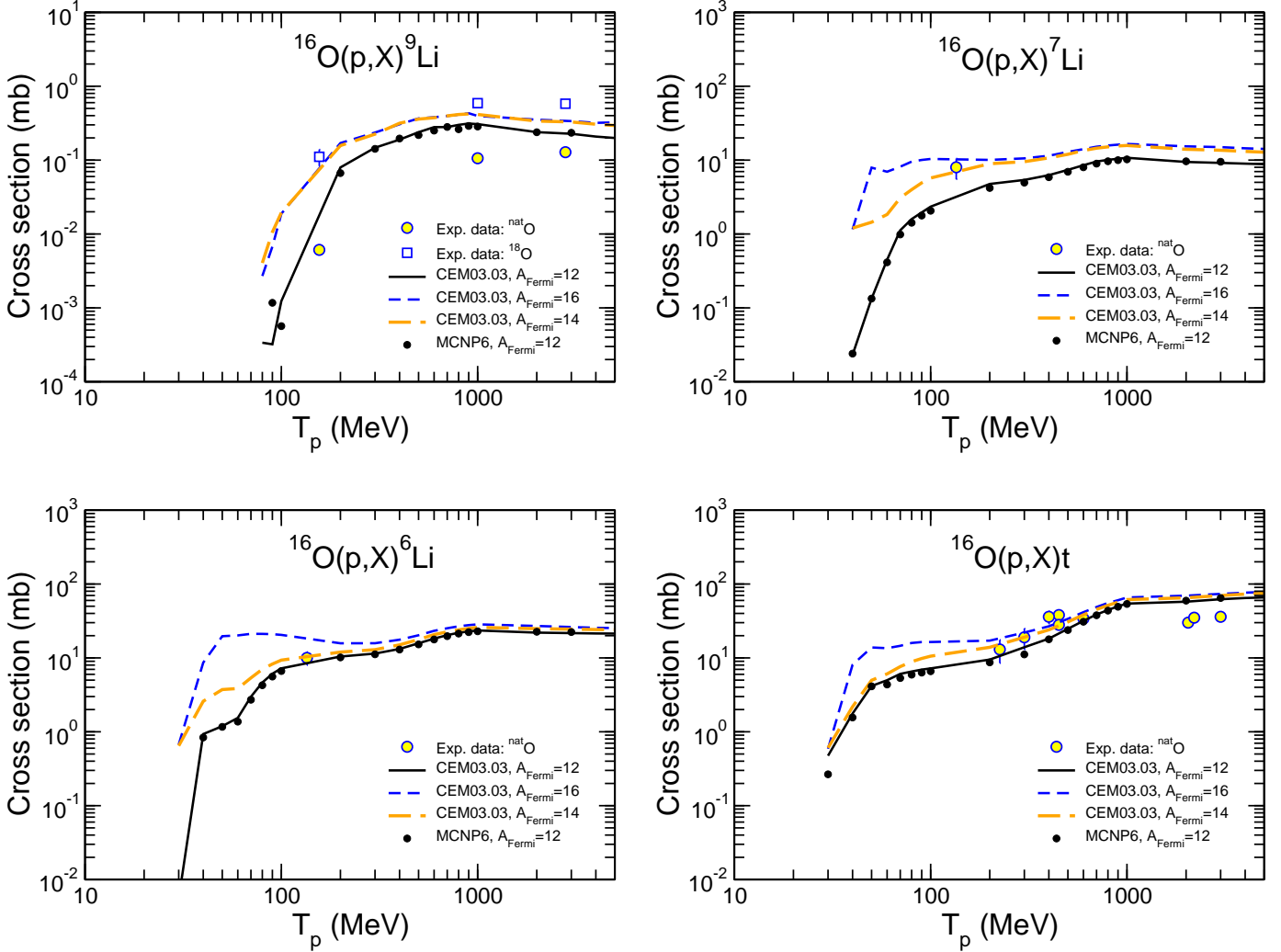


Figure 9: The same as in Fig. 7, but for the production of ${}^9\text{Li}$, ${}^7\text{Li}$, ${}^6\text{Li}$, and t .

4. Conclusion

Various fragmentation reactions induced by protons and light nuclei of energies around 1 GeV/nucleon and below on light target nuclei are studied with the latest Los Alamos Monte Carlo transport code MCNP6 and with its cascade-exciton model (CEM) and Los Alamos version of the quark-gluon string model (LAQGSM) event generators, version 03.03, used as stand-alone codes. On the whole, MCNP6 and its CEM and LAQGSM event generators describe quite well all the reactions we tested here, providing good enough agreement with available experimental data. This is especially important for calculations of cross sections of arbitrary products as functions of incident projectile energies, *i.e.*, excitation functions, one of the most difficult tasks for any nuclear reaction model. Our current results show a good prediction by MCNP6 and CEM03.03, used as a stand-alone code, of a large variety of excitation functions for products from proton-induced reactions on N, O, Al, and Si. An older version of CEM, CEM95, was able to predict reasonably well most excitation functions for medium and heavy nuclei-targets, but had big problems in calculating some

excitation functions for light nuclei [62].

CEM and LAQGSM assume that intermediate-energy fragmentation reactions on light nuclei occur generally in two stages. The first stage is the intranuclear cascade (INC), followed by the second, Fermi breakup disintegration of light excited residual nuclei produced after INC. Both CEM and LAQGSM also account for coalescence of light fragments (complex particles) up to ${}^4\text{He}$ from energetic nucleons emitted during INC.

We investigate the validity and performance of MCNP6, CEM, and LAQGSM in simulating fragmentation reactions at intermediate energies. We find that while the fixed “default” versions of CEM03.03 and LAQGSM03.03 in MCNP6 provide reasonably good predictions for all reactions tested here, a fine-tuning of the A_{Fermi} parameter in the Fermi breakup model and of momentum cut-off parameters in the coalescence model may provide a better description of some experimental data. We may consider such a fine-tuning of these and other CEM and LAQGSM parameters later, after we complete our work [59, 60] on extending the preequilibrium model in CEM and

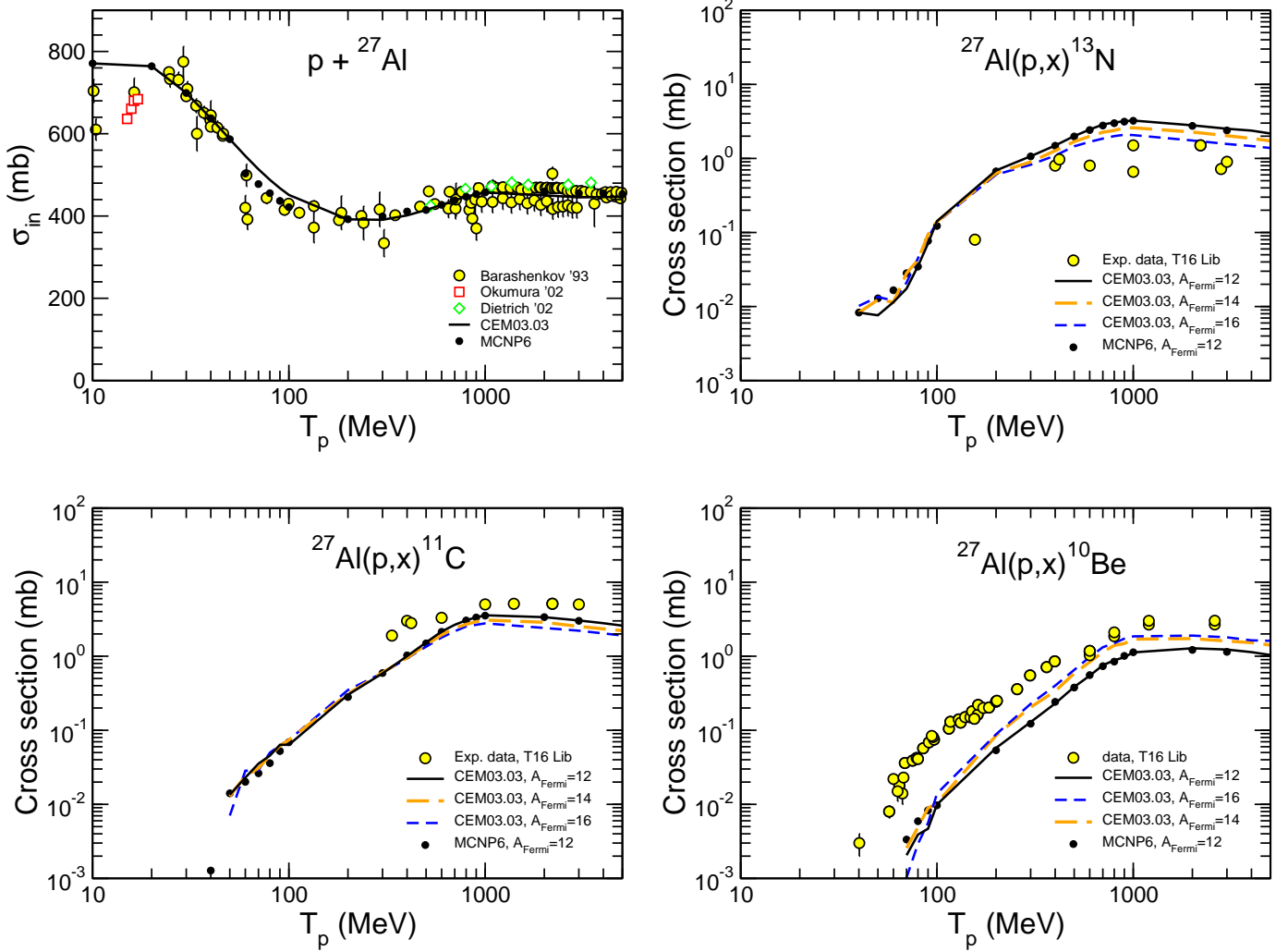


Figure 10: Total inelastic cross section and excitation functions for the production of ^{13}N , ^{11}C , and ^{10}Be , from $p + ^{27}\text{Al}$ calculated with CEM03.03 using the “standard” version of the Fermi breakup model ($A_{\text{Fermi}} = 12$) and with cut-off values for A_{Fermi} of 16 and 14, as well as with MCNP6 using CEM03.03 ($A_{\text{Fermi}} = 12$) compared with experimental data, as indicated. Experimental data for inelastic cross sections are from Refs. [39, 45, 46], while the data for excitation functions are from the T16 Lib compilation [42].

LAQGSM to account for possible emission of light fragments heavier than ^4He (up to ^{28}Mg) at this stage of reactions.

Acknowledgments

We are grateful to our colleagues, Drs. Konstantin K. Gudima and Arnold J. Sierk for a long and very fruitful collaboration with us and for several useful discussions of the results presented here.

We thank Drs. Masayaki Hagiwara, Shoji Nagamiya, Toshiya Sanami, Nikolai M. Sobolevsky, and Yusuke Uozumi for sending us their publications or/and files with numerical values of their experimental data we use in our work.

We are grateful to Drs. Lawrence J. Cox and Avneet Sood of LANL and to Prof. Akira Tokuhiro of University of Idaho for encouraging discussions and support.

Last but not least, we thank Dr. Roger L. Martz for a careful reading of our manuscript and useful suggestions on its improvement.

This study was carried out under the auspices of the National Nuclear Security Administration of the U.S. Department of Energy at Los Alamos National Laboratory under Contract No. DE-AC52-06NA253996.

This work is supported in part (for L.M.K) by the M. Hildred Blewett Fellowship of the American Physical Society, www.aps.org.

References

- [1] I. Pshenichnov, A. Botvina, I. Mishustin, W. Grainer, Nucl. Instrum. Methods B **268** (2010) 604.
- [2] M. Hultqvist, M. Lazzeroni, A. Botvina, I. Gudowska, N. Sobolevsky, A. Brahme, Phys. Med. Biol. **57** (2012) 4369.
- [3] D. C. Hansen, A. Lühr, N. Sobolevsky, N. Bassler, Phys. Med. Biol. **57** (2012) 2393.
- [4] A. Lühr, D. C. Hansen, R. Teiwes, N. Sobolevsky, O. Jäkel, N. Bassler, Phys. Med. Biol. **57** (2012) 5169.
- [5] T. Ogawa, T. Sato, S. Hashimoto, K. Niita, Nucl. Instrum. Methods A **723** (2013) 36.
- [6] T. Sato, K. Niita, N. Matsuda, S. Hashimoto, Y. Iwamoto, S. Noda, T.

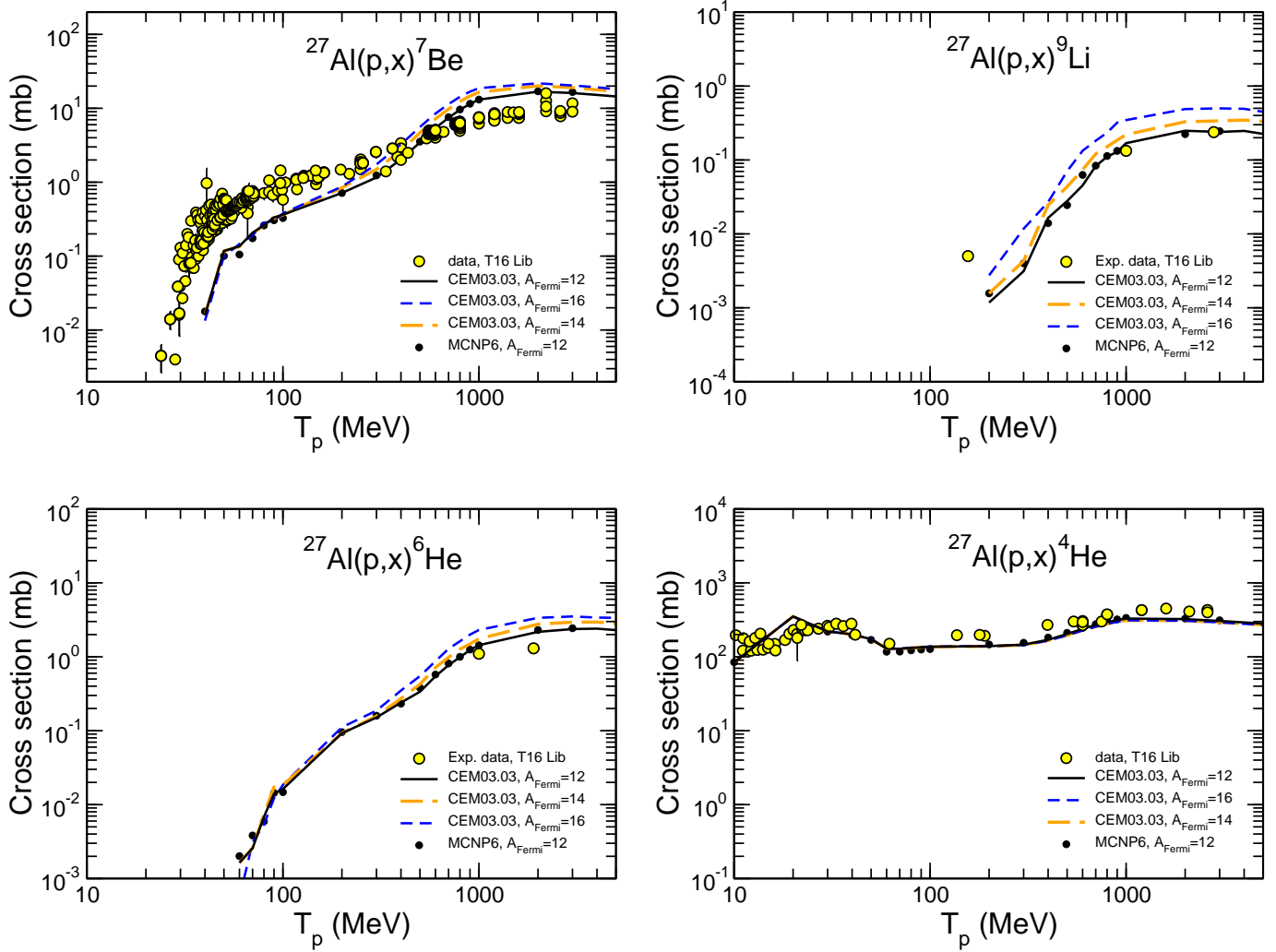


Figure 11: Excitation functions for the production of ${}^7\text{Be}$, ${}^9\text{Li}$, ${}^6\text{He}$, and ${}^4\text{He}$ from $p + {}^{27}\text{Al}$ calculated with CEM03.03 using the “standard” version of the Fermi breakup model ($A_{\text{Fermi}} = 12$) and with cut-off values for A_{Fermi} of 16 and 14, as well as with MCNP6 using CEM03.03 ($A_{\text{Fermi}} = 12$) compared with experimental data, as indicated. Experimental data are from the T16 Lib compilation [42].

- Ogawa, H. Iwase, H. Nakashima, T. Fukahori, K. Okumura, T. Kai, S. Chiba, T. Furuta, L. Sihver, J. Nucl. Sci. Technol. **50** (2013) 913.
- [7] T. Goorley, M. James, T. Booth, F. Brown, J. Bull, L. J. Cox, J. Durkee, J. Elson, M. Fensin, R. A. Forster, J. Hendricks, H. G. Hughes, R. Johns, B. Kiedrowski, R. Martz, S. Mashnik, G. McKinney, D. Pelowitz, R. Prael, J. Sweezy, L. Waters, T. Wilcox, T. Zukaitis, Nucl. Technol. **180** (2012) 298.
- [8] S. G. Mashnik, A. J. Sierk, CEM03.03 User Manual, LANL Report LA-UR-12-01364, Los Alamos (2012); <https://mcnp.lanl.gov/>.
- [9] S. G. Mashnik, K. K. Gudima, R. E. Prael, A. J. Sierk, M. I. Baznat, N. V. Mokhov, CEM03.03 and LAQGSM03.03 Event Generators for the MCNP6, MCNPX, and MARS15 Transport Codes, Invited lectures presented at the Joint ICTP-IAEA Advanced Workshop on Model Codes for Spallation Reactions, February 4-8, 2008, ICTP, Trieste, Italy, LANL Report LA-UR-08-2931, Los Alamos (2008); arXiv:0805.0751.
- [10] S. G. Mashnik, K. K. Gudima, N. V. Mokhov, R. E. Prael, LAQGSM03.03 Upgrade and Its Validation, LANL Report LA-UR-07-6198, Los Alamos (2007); arXiv:0709.1736.
- [11] S. G. Mashnik, Eur. Phys. J. Plus **126** (2011) 49; arXiv:1011.4978.
- [12] S. G. Mashnik, Validation and Verification of MCNP6 Against High-Energy Experimental Data and Calculations by Other Codes. I. The CEM Testing Primer, LANL Report LA-UR-11-05129, Los Alamos (2011); <https://mcnp.lanl.gov/>.
- [13] S. G. Mashnik, Validation and Verification of MCNP6 Against High-Energy Experimental Data and Calculations by other Codes. II. The LAQGSM Testing Primer, LANL Report LA-UR-11-05627, Los Alamos (2011); <https://mcnp.lanl.gov/>.
- [14] S. G. Mashnik, Validation and Verification of MCNP6 Against High-Energy Experimental Data and Calculations by other Codes. III. The MPI Testing Primer, LANL Report LA-UR-13-26944, Los Alamos (2013); <https://mcnp.lanl.gov/>.
- [15] K. K. Gudima, S. G. Mashnik, V. D. Toneev, JINR Communications P2-80-774 and P2-80-777, Dubna (1980); Nucl. Phys. **A401** (1983) 329.
- [16] V. S. Barashenkov, V. D. Toneev, *Interaction of High Energy Particle and Nuclei with Atomic Nuclei* (Atomizdat, Moscow, 1972) [in Russian].
- [17] V. S. Barashenkov, A. S. Il'inov, N. M. Sobolevskii, V. D. Toneev, Usp. Fiz. Nauk **109** (1073) 91 [Sov. Phys. Usp. **16** (1973) 31].
- [18] K. K. Gudima, G. A. Ososkov, V. D. Toneev, Sov. J. Nucl. Phys. **21** (1975) 138.
- [19] S. G. Mashnik, V. D. Toneev, MODEX - the Program for Calculation of the Energy Spectra of Particles Emitted in the Reactions of Pre-Equilibrium and Equilibrium Statistical Decays [text in Russian, code in FORTRAN66], JINR Communication P4-8417, Dubna (1974); LA-UR-12-20390 (2012 LANL reprint); <https://mcnp.lanl.gov/>.
- [20] K. K. Gudima, S. G. Mashnik, A. J. Sierk, User Manual for the code LAQGSM, LANL Report LA-UR-01-6804, Los Alamos (2001);

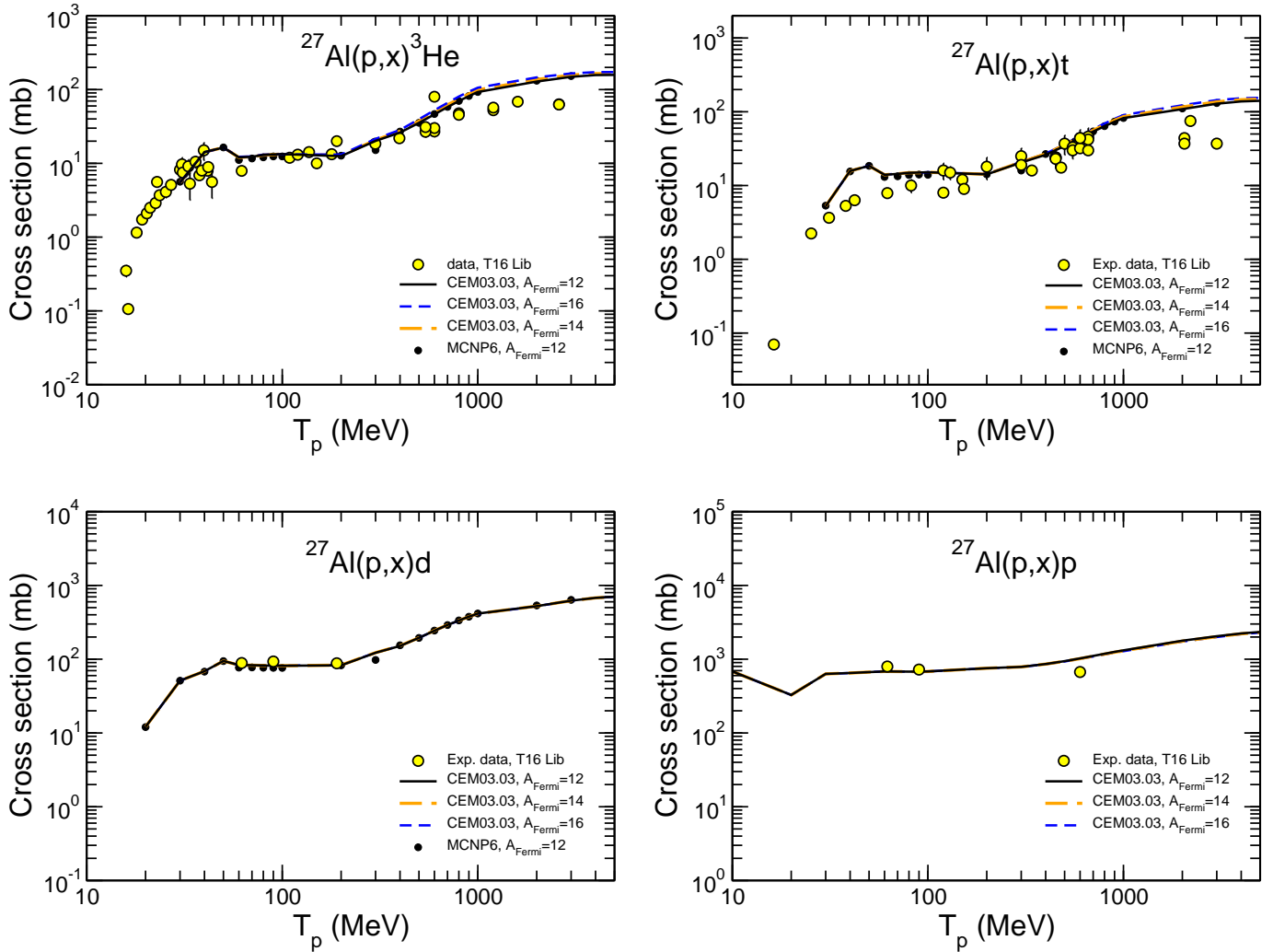


Figure 12: The same as in Fig. 11, but for the production of ${}^3\text{He}$, t, d, and p.

- <https://mcnp.lanl.gov/>.
- [21] N. S. Amelin, K. K. Gudima, V. D. Toneev, *Sov. J. Nucl. Phys.* **51** (1990) 327.
- [22] S. G. Mashnik, K. K. Gudima, A. J. Sierk, M. I. Baznat, N. V. Mokhov, CEM03.01 User Manual, LANL Report LA-UR-05-7321, Los Alamos (2005); <https://mcnp.lanl.gov/>.
- [23] S. G. Mashnik, K. K. Gudima, M. I. Baznat, A. J. Sierk, R. E. Prael, N. V. Mokhov, CEM03.01 and LAQGSM03.01 Versions of the Improved Cascade-Exciton Model (CEM) and Los Alamos Quark-Gluon String Model (LAQGSM) Codes, LANL Report LA-UR-05-2686, Los Alamos (2005); <https://mcnp.lanl.gov/>.
- [24] V. S. Barashenkov, K. K. Gudima, V. D. Toneev, *JINR Communications P2-4065 and P2-4066*, Dubna, 1968.
- [25] K. K. Gudima, S. G. Mashnik, Extension of the LAQGSM03 Code to Describe Photo-Nuclear Reactions up to Tens of GeV, in: *Proc. 11th Int. Conf. on Nuclear Reaction Mechanisms, Varenna, Italy, 2006*, edited by E. Gadioli (University of Milan, 2006), pp. 525-534; arXiv:nucl-th/0607007.
- [26] V. D. Toneev, K. K. Gudima, *Nucl. Phys.* **A400** (1983) 173c.
- [27] N. S. Amelin, K. K. Gudima, V. D. Toneev, *Sov. J. Nucl. Phys.* **51** (1990) 1093 [*Yad. Fiz.* **51** (1990) 1730]; *ibid.*, **52** (1990) 172 [*Yad. Fiz.* **52** (1990) 272]; A. B. Kaidalov, *Sov. J. Nucl. Phys.* **45** (1987) 902 [*Yad. Fiz.* **45** (1987) 1452]; N. S. Amelin, Simulation of Nuclear Collisions at High Energy in the Framework of the Quark-Gluon String Model, *JINR Communication 86-802*, Dubna (1986); N. S. Amelin, V. S. Barashenkov, N. V. Slavin, *Sov. J. Nucl. Phys.* **40** (1984) 991 [*Yad. Fiz.* **40** (1984) 1560].
- [28] A. S. Iljinov, I. A. Pshenichnov, N. Bianchi, E. De Sanctis, V. Muccifora, M. Mirazita, P. Rossi, *Nucl. Phys.* **A616** (1997) 575.
- [29] S. G. Mashnik, M. I. Baznat, K. K. Gudima, A. J. Sierk, R. E. Prael, *J. Nucl. Radiochem. Sci.* **6** (2005) A1; arXiv:nucl-th/0503061.
- [30] C. Kalbach, *Phys. Rev. C* **37** (1988) 2350.
- [31] S. G. Mashnik, A. J. Sierk, CEM2k - Recent Developments in CEM, in: *Proc. AccApp00, 2000, Washington, DC, USA*, ANS, La Grange Park, IL, USA, 2001, p. 328; arXiv:nucl-th/0011064.
- [32] M. Veselsky, *Nucl. Phys.* **A705** (2002) 193.
- [33] S. Furihata, *Nucl. Instrum. Methods B* **171** (2000) 252; *J. Nucl. Sci. Technol. Suppl.* **2** (2002) 758; Ph.D. thesis, Tohoku University, March, 2003.
- [34] F. Atchison, Spallation and Fission in Heavy Metal Nuclei under Medium Energy Proton Bombardment, in: *Proc. Meeting on Targets for Neutron Beam Spallation Source, Julich, June 11-12, 1979*, edited by G. S. Bauer, (Jul-Conf-34, Julich GmbH, Germany, 1980) p. 17; *Nucl. Instrum. Methods B* **259** (2007) 909.
- [35] M. Baznat, K. Gudima, S. Mashnik, Proton-Induced Fission Cross Section Calculation with the LANL Codes CEM2k+GEM2 and LAQGSM+GEM2, in: *Proc. AccApp03, San Diego, California, June 1-5, 2003*, (ANS, La Grange Park, IL 60526, USA, 2004), p. 976; arXiv:nucl-th/0307014.
- [36] S. G. Mashnik, A. J. Sierk, R. E. Prael, MCNP6 Fission Cross Section Calculation at Intermediate and High Energies, in: *Proc. 2013 Int. Conf. on Nuclear Data for Sci. & Technol. (ND2013)*, March 4-8, 2013, New

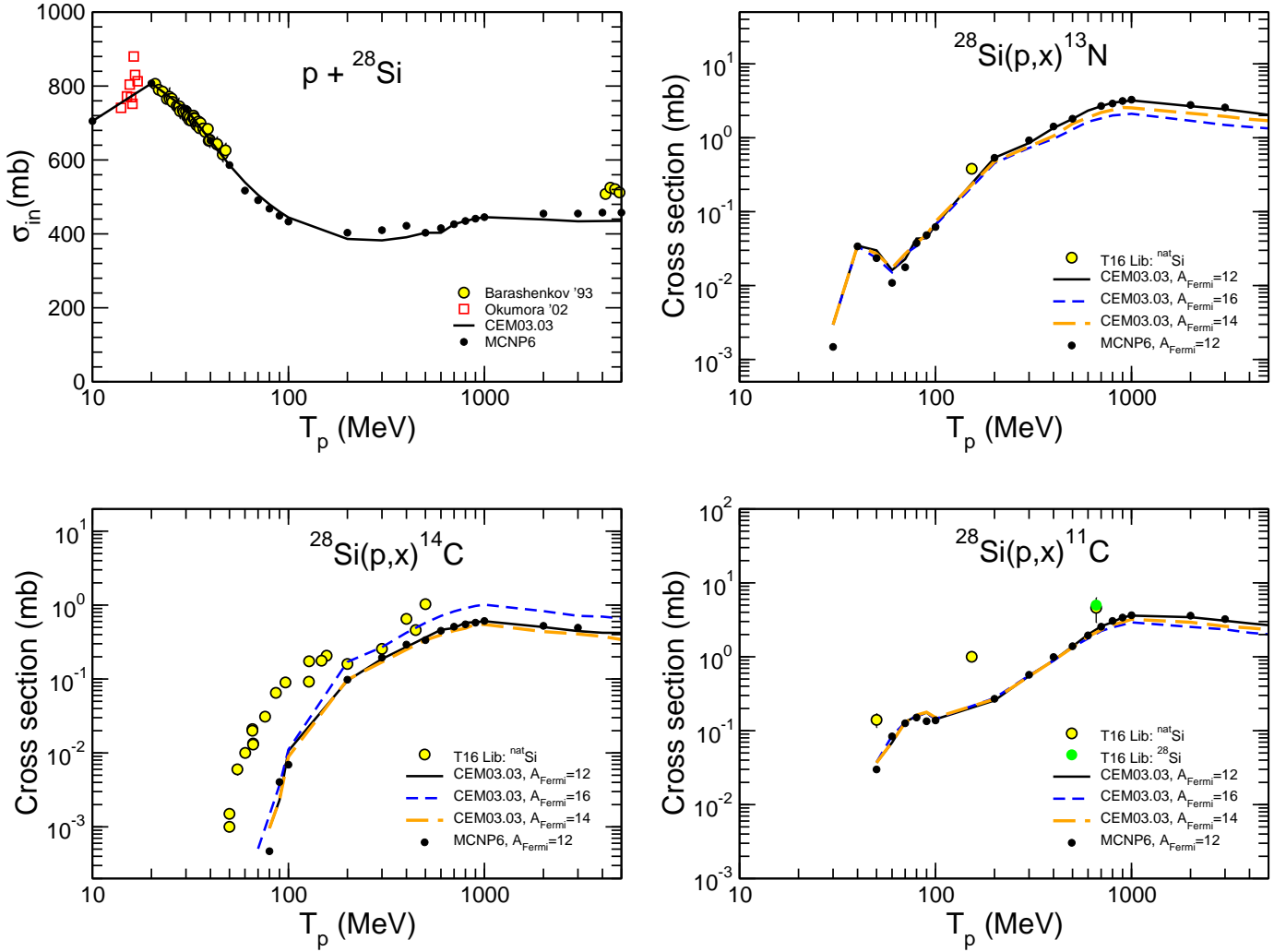


Figure 13: Total inelastic cross section and excitation functions for the production of ^{13}N , ^{14}C , and ^{11}C , from $p + ^{28}\text{Si}$ calculated with CEM03.03 using the “standard” version of the Fermi breakup model ($A_{\text{Fermi}} = 12$) and with cut-off values for A_{Fermi} of 16 and 14, as well as with MCNP6 using CEM03.03 ($A_{\text{Fermi}} = 12$) compared with experimental data, as indicated. Experimental data for inelastic cross sections are from Refs. [39, 45], while the data for excitation functions are from the T16 Lib compilation [42].

- York, USA, Nuclear Data Sheets, 2014; arXiv:1303.4308.
- [37] E. Fermi, *Prog. Theor. Phys.* **5** (1950) 570.
- [38] N. Amelin, *Physics and Algorithms of the Hadronic Monte-Carlo Event Generators*. Notes for a developer, CERN/IT/ASD Report CERN/IT/99/6, Geneva, Switzerland and JINR LHE, Dubna, Russia (1998); http://www.infocern.ch/asd/geant/geant4_public/G4UsersDocuments/Overview/html/index.html/.
- [39] V. S. Barashenkov, *Cross Sections of Interaction of Particles and Nuclei with Nuclei*, (in Russian) JINR, Dubna (1993); see tabulated data at: <http://www.nea.fr/html/dbdata/bara.html>.
- [40] R. F. Carlson, A. J. Cox, T. N. Nasr, M. S. De Jong, D. L. Ginther, D. K. Hasell, A. M. Sourkes, W. T. H. Van Oers, D. J. Margaziotis, *Nucl. Phys.* **A445** (1985) 57.
- [41] A. E. Taylor and E. Wood, *Nucl. Phys.* **25** (1961) 642.
- [42] S. G. Mashnik, A. J. Sierk, K. A. Van Riper, and W. B. Wilson, *Production and Validation of Isotope Production Cross Section Libraries for Neutrons and Protons to 1.7 GeV*, LANL Report LA-UR-98-6000 (1998); in: *Proc. SARE-4, Knoxville, TN, September 13-16, 1998* (ORNL, 1999, pp. 151-162); arXiv:nucl-th/9812071; our T-16 Library “T-16 Lib” is updated permanently when new experimental data became available to us.
- [43] A. Ingemarsson, J. Nyberg, P. U. Renberg, O. Sundberg, R. F. Carlson, A. Auce, R. Johansson, G. Tibell, B. C. Clark, L. K. Kerr, S. Hama, *Nucl. Phys.* **A653** (1999) 341.
- [44] R. F. Carlson, A. J. Cox, J. R. Nimmo, N. E. Davison, S. A. Elbaker, J. L. Horton, A. Houdayer, A. M. Sourkes, W. T. H. van Oers, D. J. Margaziotis, *Phys. Rev. C* **12** (1975) 1167.
- [45] N. Okumura, Y. Aoki, T. Joh, Y. Honkyu, K. Hirota, K. S. Itoh, *Nucl. Instrum. Methods A* **487** (2002) 565.
- [46] F. S. Dietrich, E. P. Hartouni, S. C. Johnson, G. J. Schmid, R. Soltz, W. P. Abfalterer, R. C. Haight, L. S. Waters, A. L. Hanson, R. W. Finlay, G. S. Blanpied, *J. Nucl. Sci. Technol. Suppl.* **2** (2002) 269.
- [47] W. R. Webber, J. C. Kish, D. A. Schrier, *Phys. Rev. C* **41** (1990) 547.
- [48] C. Zeitlin, J. Miller, S. Guetersloh, L. Heilbronn, A. Fukumura, Y. Iwata, T. Murakami, S. Blattmig, R. Norman, S. Mashnik, *Phys. Rev. C* **83** (2011) 034909.
- [49] C. Zeitlin, A. Fukumura, L. Heilbronn, Y. Iwata, J. Miller, T. Murakami, *Phys. Rev. C* **64** (2001) 024902.
- [50] J. W. Wilson, J. L. Shinn, L. W. Townsend, R. K. Tripathi, F. F. Badavi, S. Y. Chun, *Nucl. Instrum. Methods B* **94** (1994) 95.
- [51] B. S. Nilsen, C. J. Waddington, J. R. Cummings, T. L. Garrard, J. Klarman, *Phys. Rev. C* **52** (1995) 3277.
- [52] F. A. Cucinotta, J. W. Wilson, R. K. Tripathi, L. W. Townsend, *Adv. Space Res.* **22** (1998) 533.
- [53] R. E. L. Green, R. G. Korteling, J. M. D’Auria, K. P. Jackson, R. L.

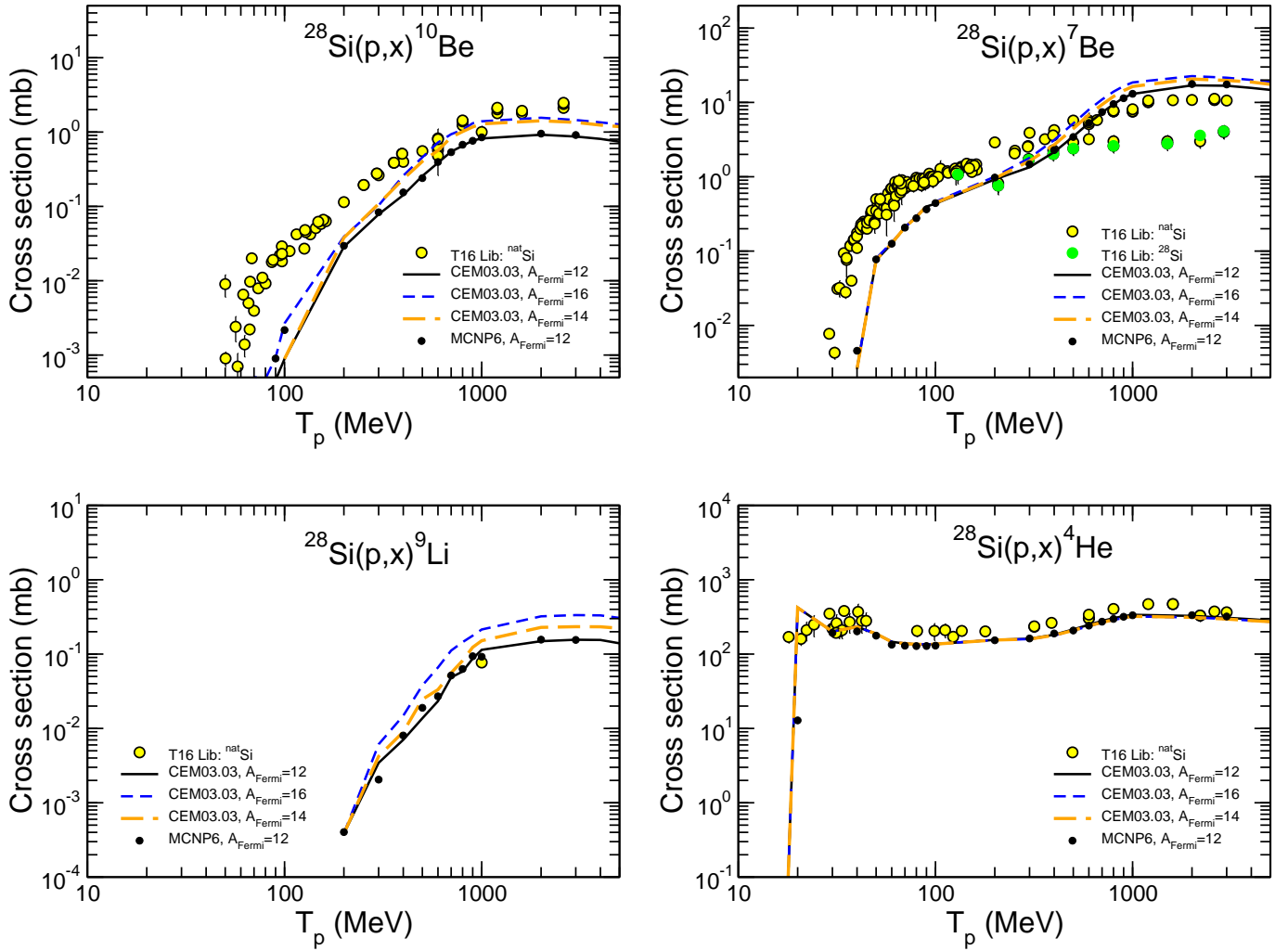


Figure 14: Excitation functions for the production of ^{10}Be , ^7Be , ^9Li , and ^4He from $p + ^{28}\text{Si}$ calculated with CEM03.03 using the “standard” version of the Fermi breakup model ($A_{\text{Fermi}} = 12$) and with cut-off values for A_{Fermi} of 16 and 14, as well as with MCNP6 using CEM03.03 ($A_{\text{Fermi}} = 12$) compared with experimental data, as indicated. Experimental data are from the T16 Lib compilation [42].

- Helmer, Phys. Rev. C **35** (1987) 1341.
- [54] Y. Uozumi, P. Evtoukhovitch, H. Fukuda, M. Imamura, H. Iwamoto, V. Kalinikov, W. Kallies, N. Khumutov, T. Kin, N. Koba, Y. Koba, N. Kuchinski, A. Moisenko, D. Mzavia, M. Nakano, V. Samoilov, Z. Tsamalaidze, G. Wakabayashia, Y. Yamashita, Nucl. Instrum. Methods A **571** (2007) 743; tabulated data are available at: http://www.qpn.kyushu-u.ac.jp/lab1/data_library.html.
- [55] M. Hagiwara, T. Sanami, T. Oishi, M. Baba, M. Takada, J. Nucl. Sci. Technol. **49** (2012) 571.
- [56] T. Sanami, M. Hagiwara, H. Iwase, M. Takada, D. Satoh, Y. Iwamoto, S. Kunieda, H. Yashima, A. Tamii, M. Baba, J. Korean Phys. Society **59** (2011) 1805.
- [57] M.-C. Lemaire, S. Nagamiya, O. Chamberlain, G. Shapiro, S. Schnetzer, H. Steiner, I. Tanihata, Tables of Light-Fragment Inclusive Cross Sections in Relativistic Heavy Ion Collisions. Part I, Lawrence Berkeley Laboratory Report LBL-8463 (1978).
- [58] S. Nagamiya, M.-C. Lemaire, E. Moeller, S. Schnetzer, G. Shapiro, H. Steiner, I. Tanihata, Phys. Rev. C **24** (1981) 971.
- [59] L. M. Kerby, S. G. Mashnik, A. J. Sierk, Preequilibrium Emission of Light Fragments in Spallation Reactions, in: *Proc. 2013 Int. Conf. on Nuclear Data for Sci. & Technol. (ND2013)*, March 4-8, 2013, New York, USA, Nuclear Data Sheets, 2014; arXiv:1303.4311.
- [60] S. G. Mashnik, L. M. Kerby, K. K. Gudima, A. J. Sierk, Extension of the CEM and LAQGSM Models to Describe Production of Energetic Light Fragments in Spallation Reactions, in: *Proc. 25th Int. Nucl. Phys. Conf. (INPC 2013), Firenze (Italy), June 2-7, 2013*, EPJ Web of Conferences **66** (2014) 03059; arXiv:1306.6547.
- [61] H. Machner, D. G. Aschman, K. Baruth-Ram, J. Carter, A. A. Cowley, F. Goldenbaum, B. M. Nangu, J. V. Pilcher, E. Sideras-Haddad, J. P. F. Sellschop, F. D. Smit, B. Spoelstra, D. Steyn, Phys. Rev. C **73** (2006) 044606.
- [62] S. G. Mashnik, A. J. Sierk, O. Bersillon, T. Gabriel, Cascade-Exciton Model Detailed Analysis of Proton Spallation at Energies from 10 MeV to 5 GeV, LANL Report LA-UR-97-97-2905, Los Alamos (1997); <https://mcnp.lanl.gov/>; Nucl. Instrum. Methods A **414** (1998) 68.

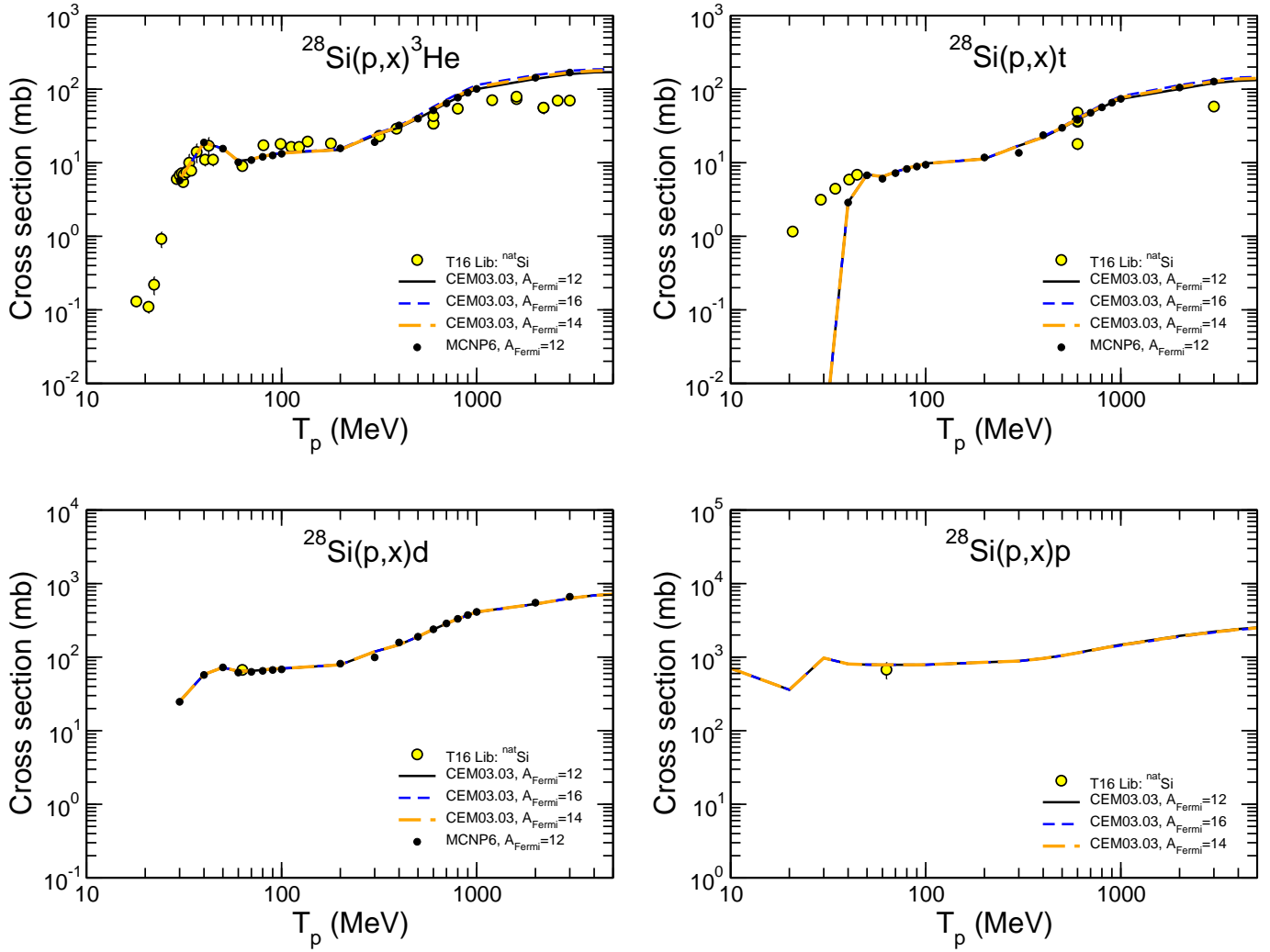


Figure 15: The same as in Fig. 14, but for the production of ^3He , t, d, and p.

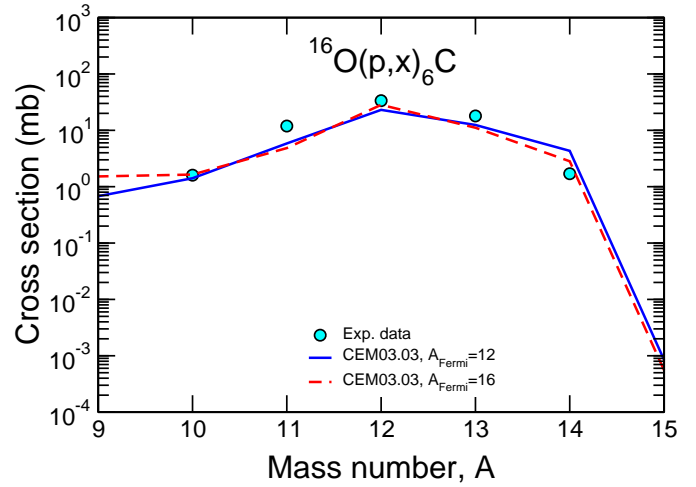
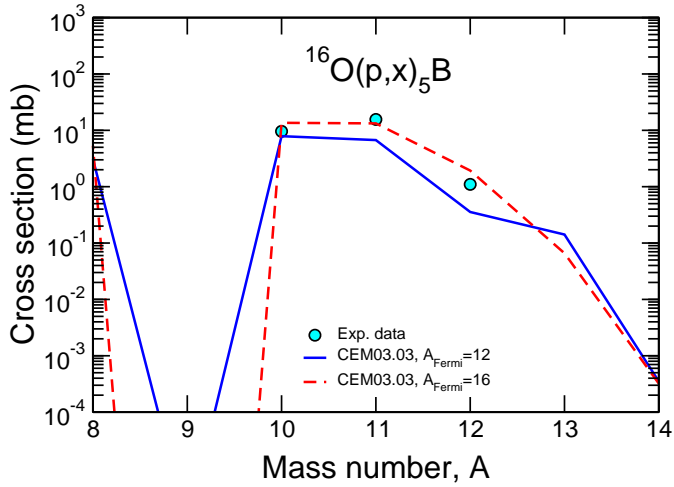
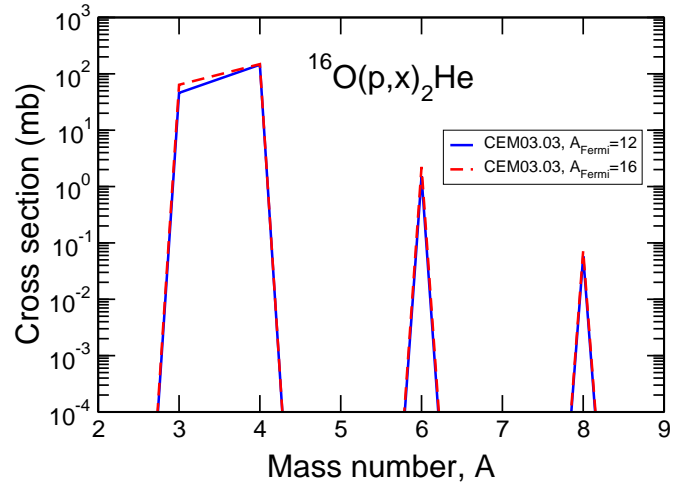
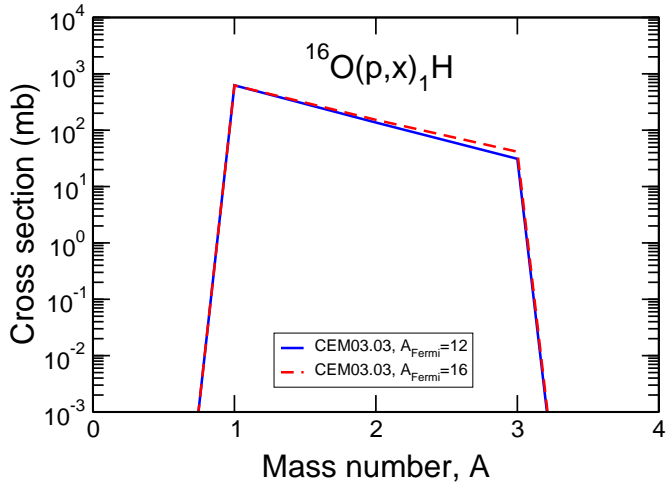


Figure 16: Examples of measured particle and LF production cross sections from $p + ^{16}\text{O}$ at 600 MeV [47] (symbols) compared with our CEM results for a Fermi breakup cut-off of $A \leq 16$ and $A \leq 12$, as indicated. All the LF from these reactions are calculated by CEM either as final products (residual nuclei) after all possible stages of reaction or via Fermi breakup after INC (Fermi breakup is used for nuclei with $A < 13$ or $A < 17$ instead of using preequilibrium emission and/or evaporation of particles).

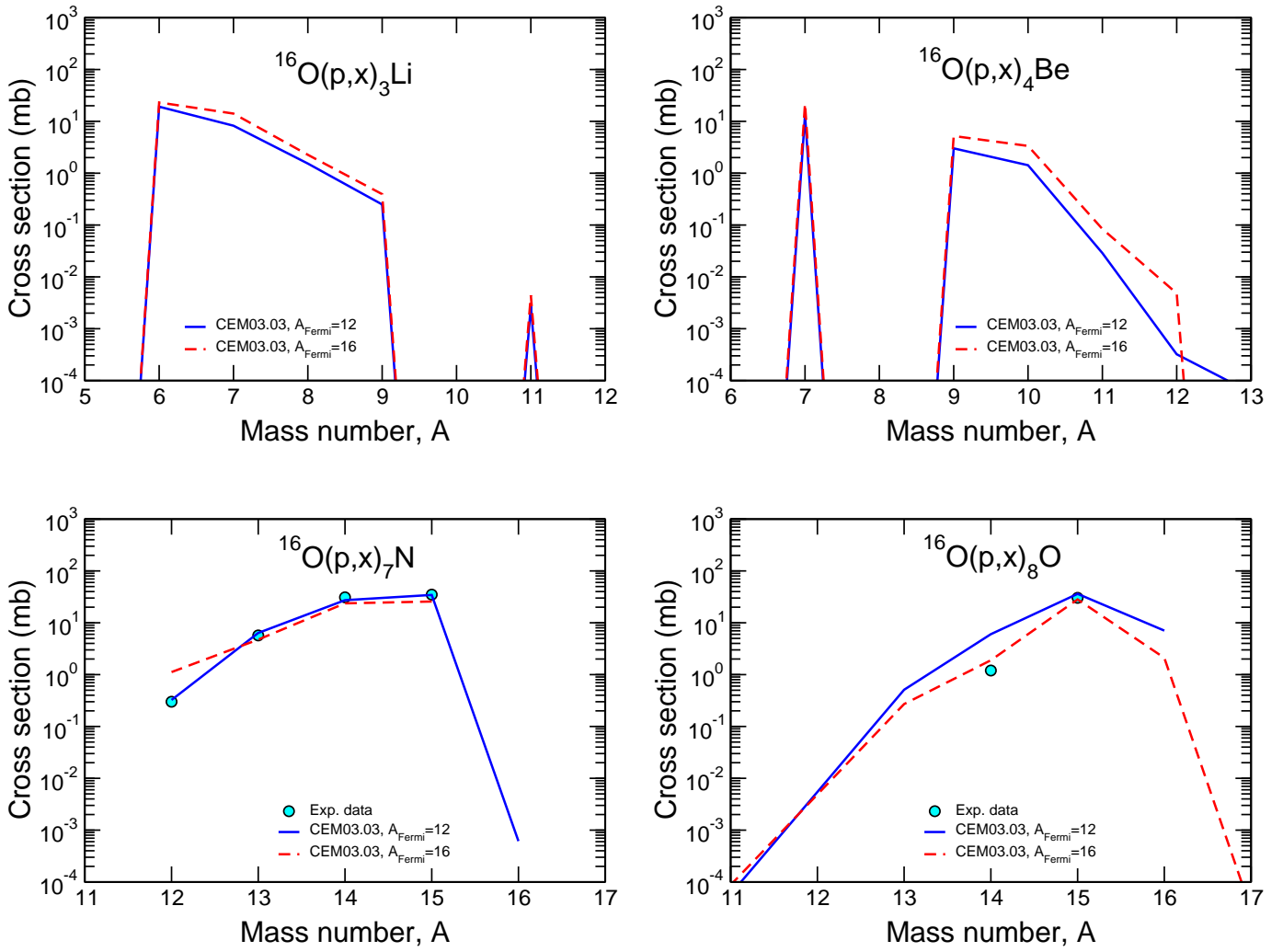


Figure 17: The same as in Fig. 16, but for the production of Li, Be, N, and O isotopes.

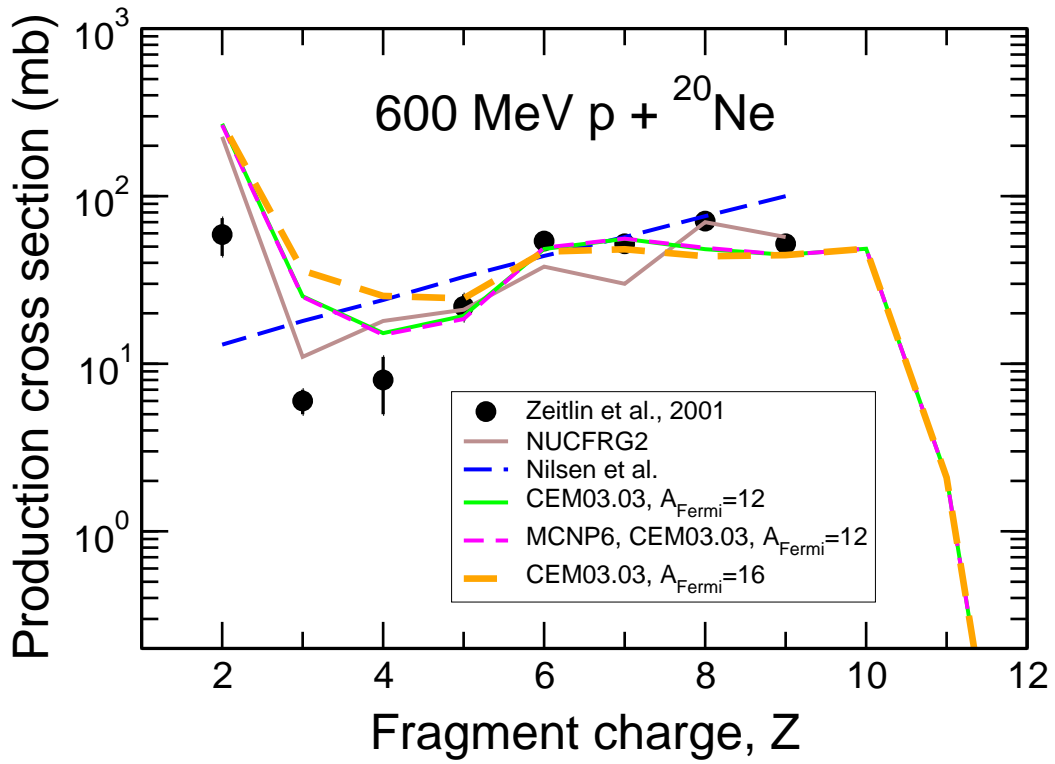


Figure 18: Atomic-number dependence of the fragment-production cross sections from the interactions of ^{20}Ne of 600 MeV/nucleon with H. Experimental data (circles) are by Zeitlin et al. [49]. For comparison, results by the NASA semi-empirical nuclear fragmentation code NUCFRG2 [50] and from a parameterization by Nilsen et al. [51] taken from Tab. III of Ref. [49] are shown as well, as indicated. Our results by CEM03.03 using the “standard” version of the Fermi breakup model ($A_{\text{Fermi}} = 12$) and $A_{\text{Fermi}} = 16$, as well as MCNP6 calculations using CEM03.03 ($A_{\text{Fermi}} = 12$) are plotted with different lines, as indicated.

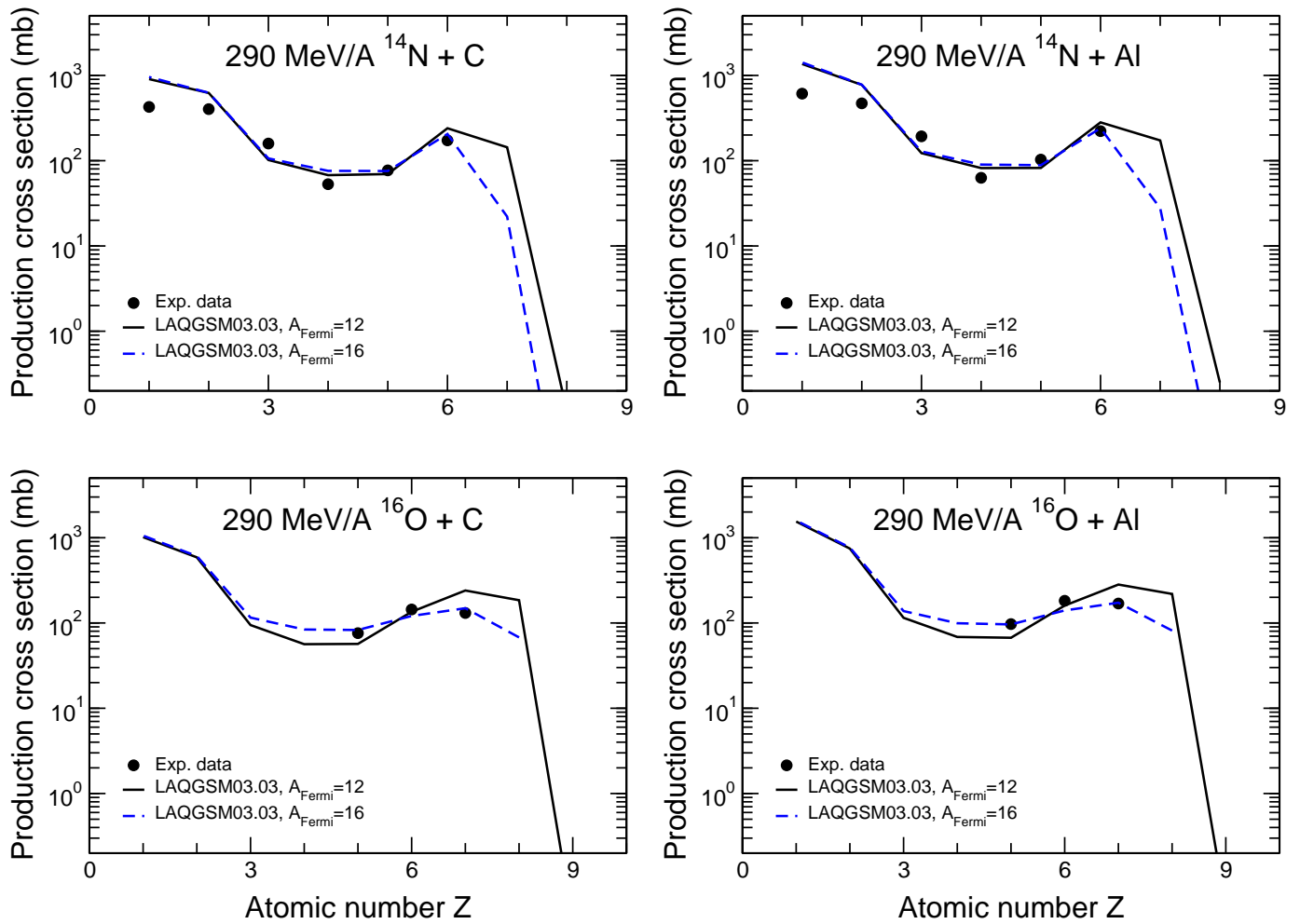


Figure 19: Atomic-number dependence of the fragment-production cross sections from the interactions of 290 MeV/nucleon ¹⁴Ne and ¹⁶O with C and Al. Experimental data (circles) are by Zeitlin et al. [48]. Our results by LAQGS03.03 using the “standard” version of the Fermi breakup model ($A_{Fermi} = 12$) are shown with solid lines, and for a cut-off value for A_{Fermi} of 16, with dashed lines, as indicated.

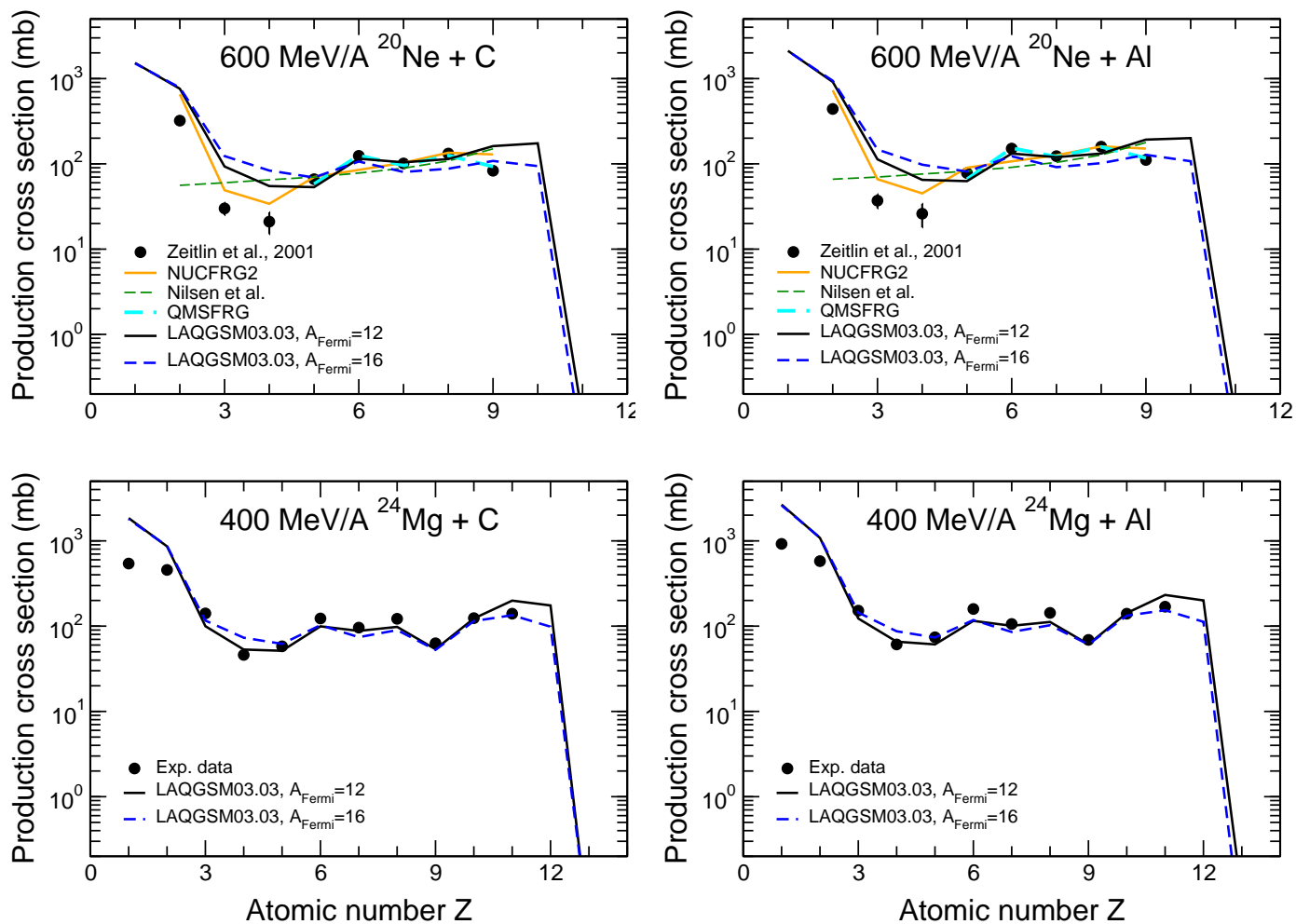


Figure 20: Atomic-number dependence of the fragment-production cross sections from the interactions of 600 MeV/nucleon ^{20}Ne with C and Al, and 400 MeV/nucleon ^{24}Mg with C and Al. Experimental data (circles) are by Zeitlin et al. [48, 49]. For comparison, at 600 MeV/A, results by the NASA semi-empirical nuclear fragmentation code NUCFRG2 [50] and the microscopic abrasion-ablation model QMSFRG [52], as well as from a parameterization by Nilsen et al. [51] taken from Tabs. III and IV of Ref. [49] are shown with different lines, as indicated. Our results by LAQGS03.03 using the “standard” version of the Fermi breakup model ($A_{\text{Fermi}} = 12$) are shown with solid lines, and for a cut-off value for A_{Fermi} of 16, with dashed lines, as indicated.

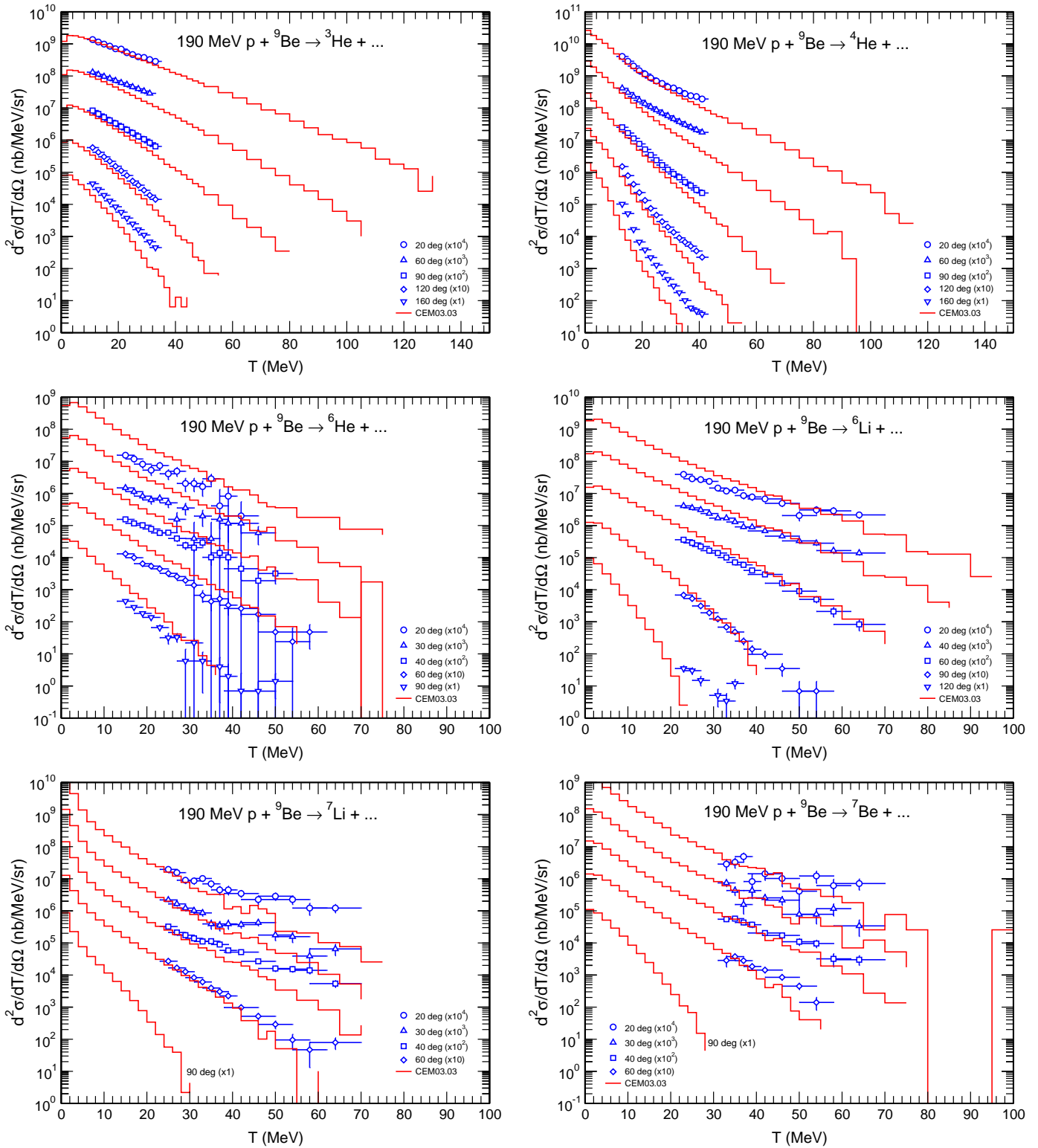


Figure 21: Examples of measured particle and LF double-differential spectra from $p + {}^9\text{Be}$ at 190 MeV [53], compared with our CEM results (histograms).

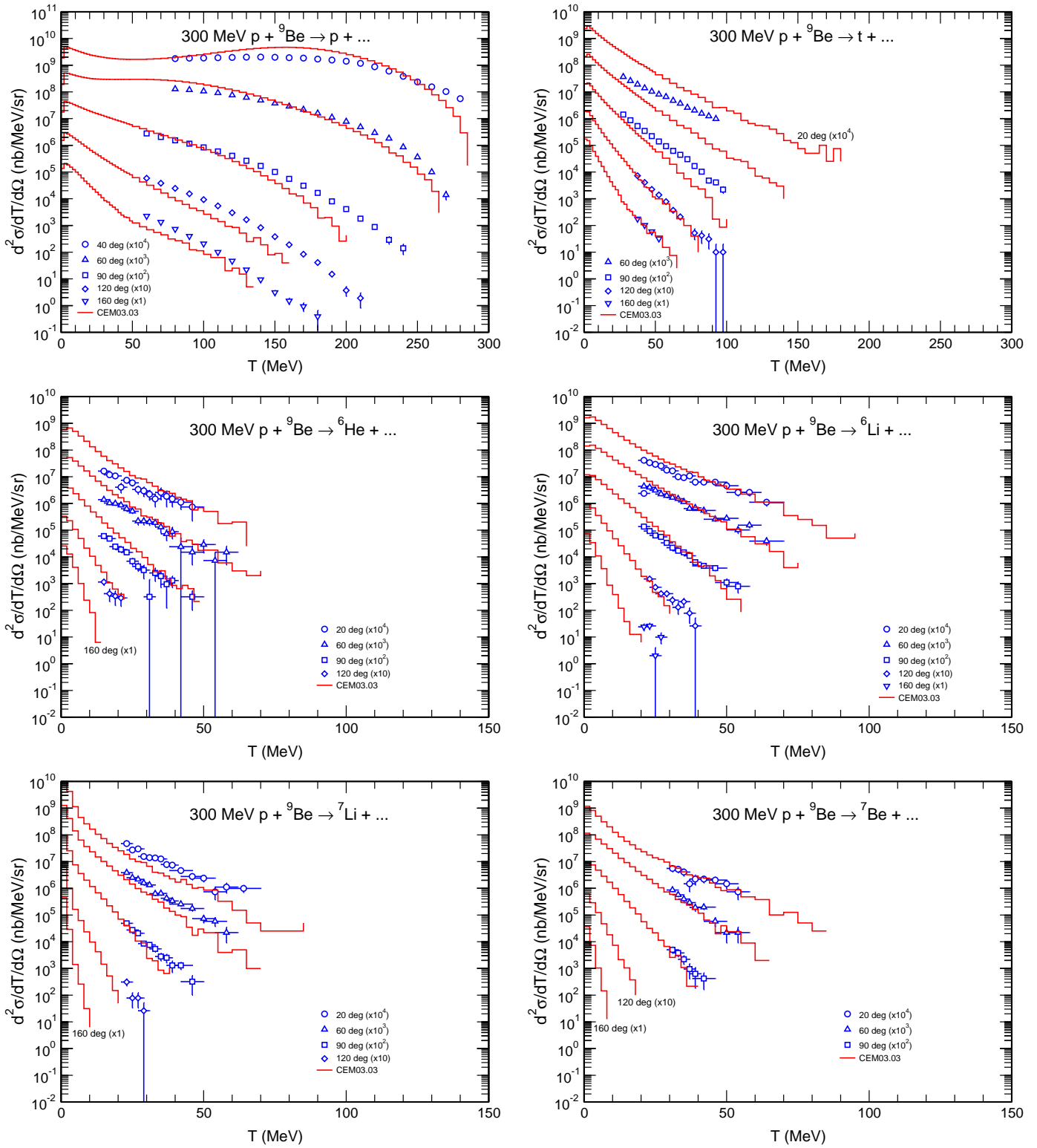


Figure 22: Examples of measured particle and LF double-differential spectra from $p + {}^9\text{Be}$ at 300 MeV [53], compared with our CEM results (histograms).

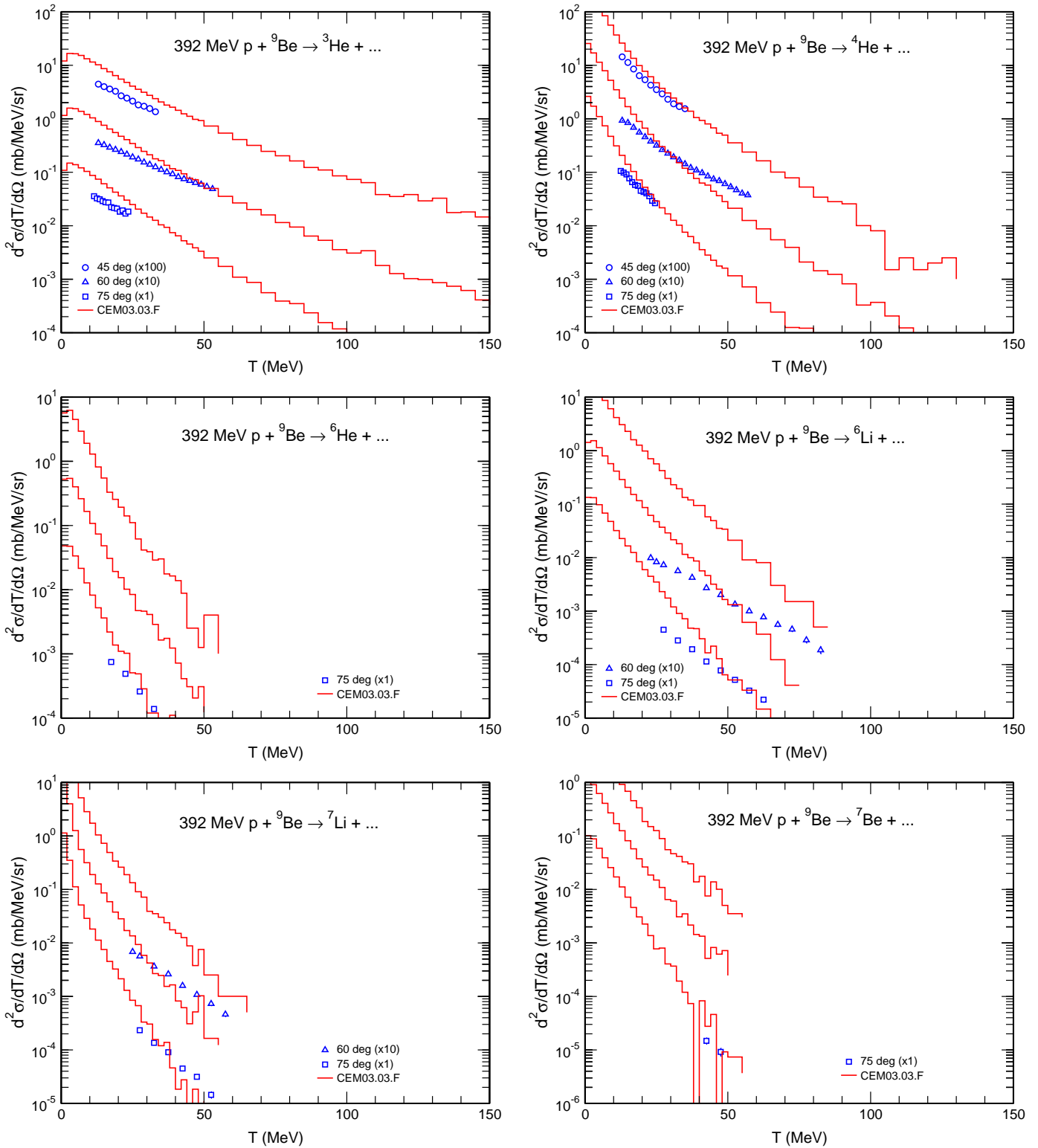


Figure 23: Examples of measured particle and LF double-differential spectra from $p + {}^9\text{Be}$ at 392 MeV [54], compared with our CEM results (histograms).

70 MeV p + ^{nat}C → ...

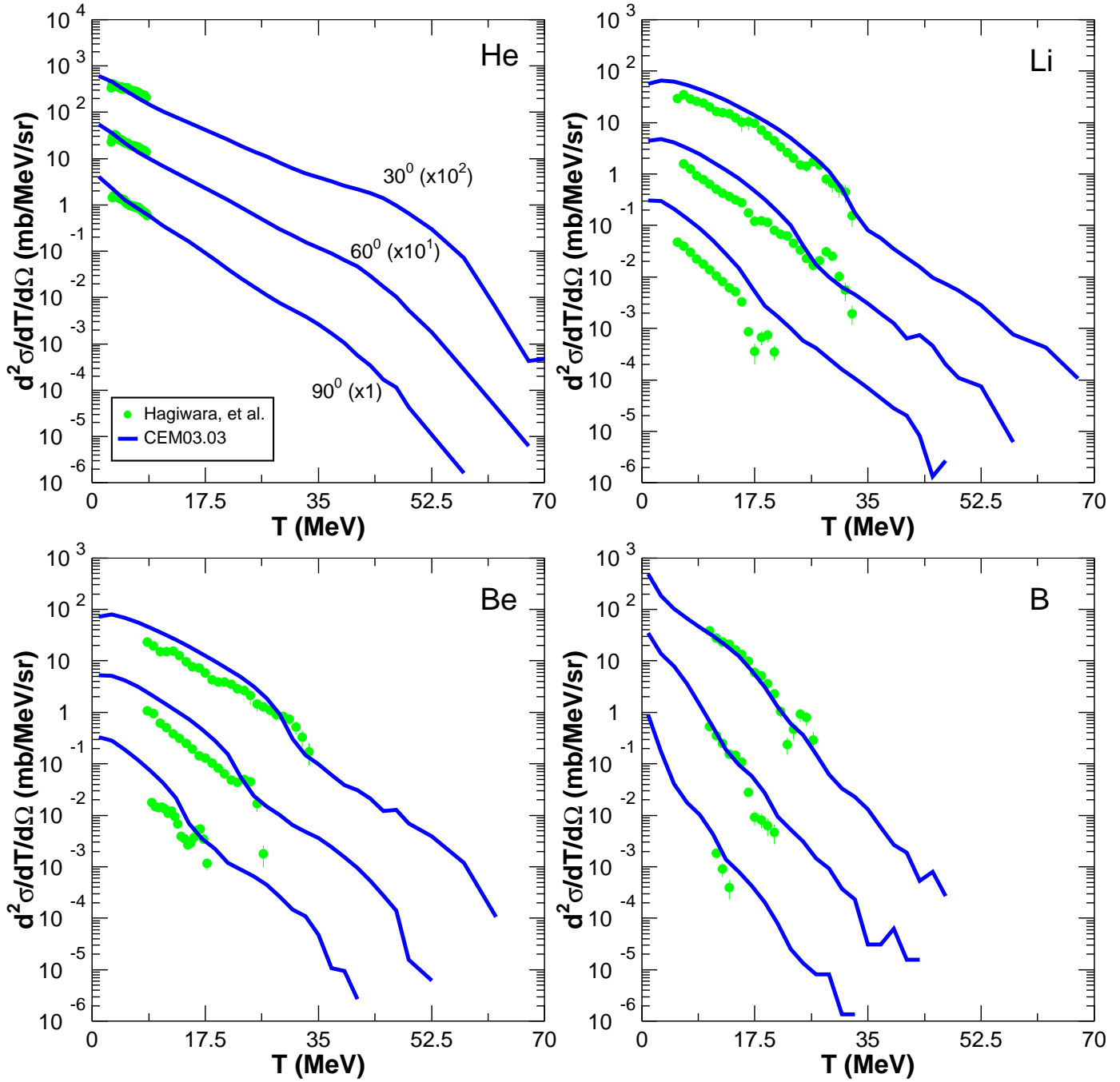


Figure 24: Comparison of CEM03.03 (solid lines) He, Li, Be, and B spectra from 70 MeV p + C with experimental data by Hagiwara et al. [55] (circles) for a natural carbon target. Our calculations were performed for ^{12}C .

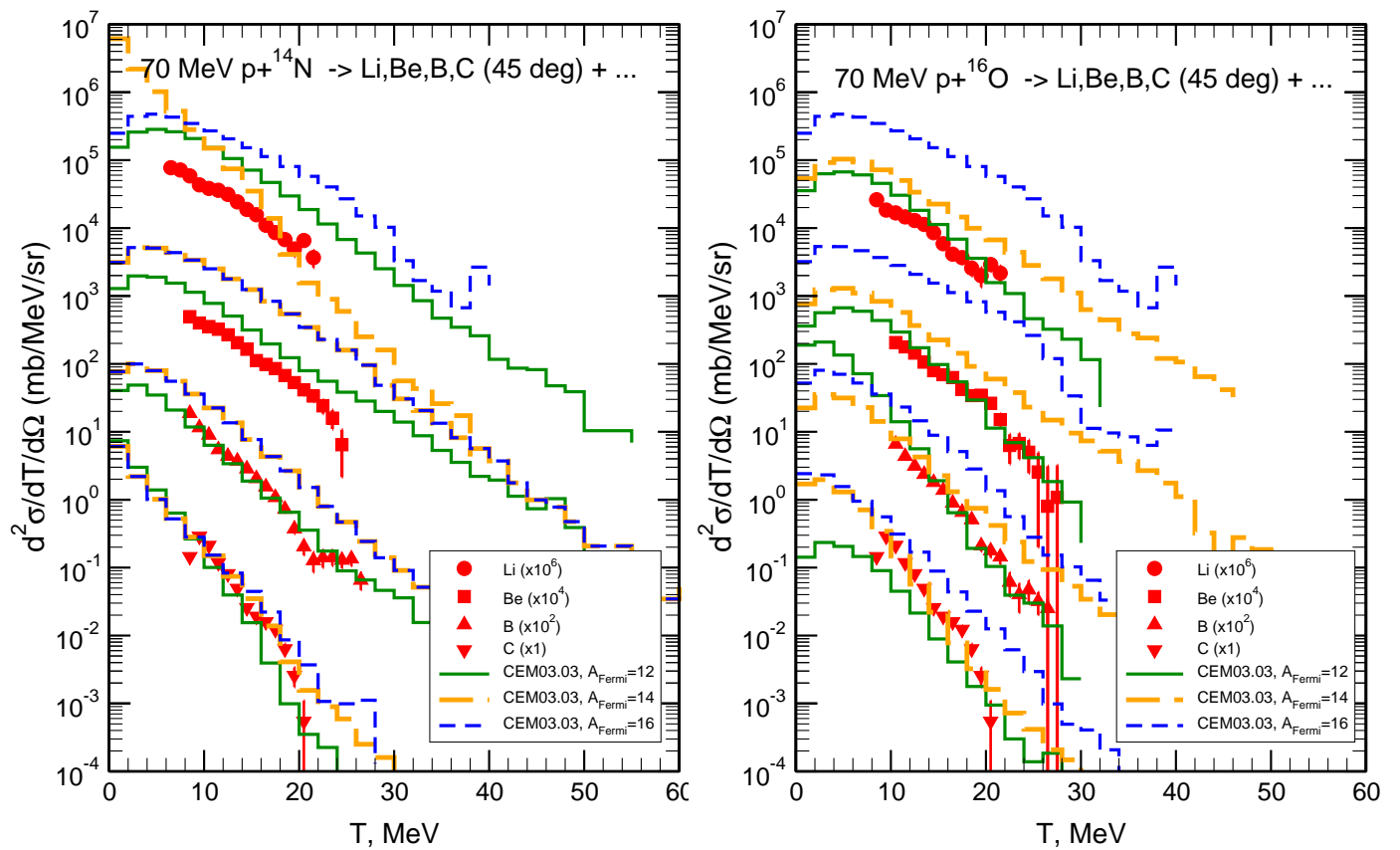


Figure 25: Comparison of Li, Be, B, and C spectra at 45 degrees from 70 MeV $p + {}^{14}\text{N}$ and ${}^{16}\text{O}$ measured by Sanami et al. [56] (symbols) with calculations by CEM03.03 using the “standard” version of the Fermi breakup model ($A_{\text{Fermi}} = 12$; solid histograms) and with cut-off values for A_{Fermi} of 16 (dashed histograms) and 14 (long-dashed histograms), as indicated.

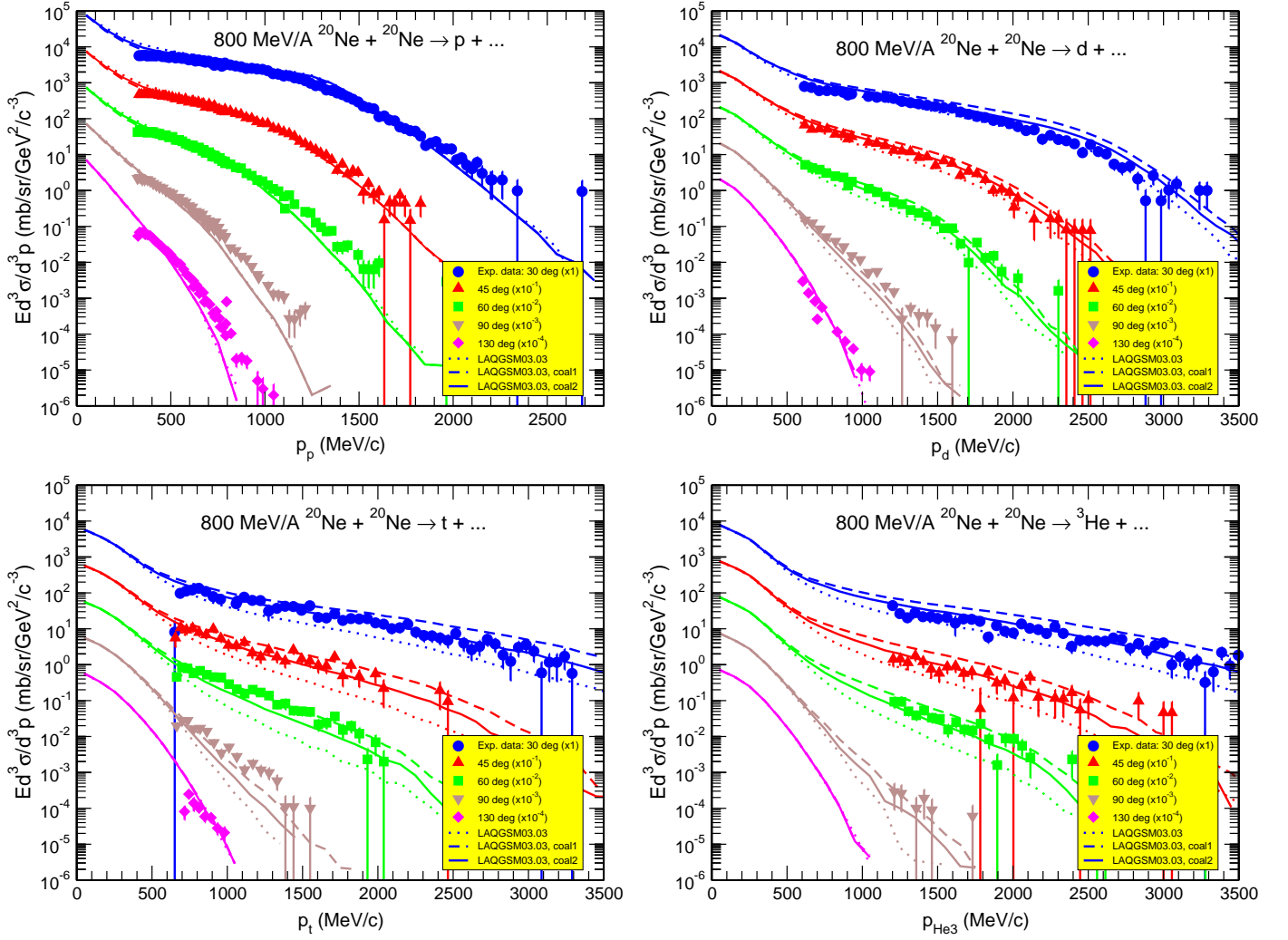


Figure 26: Comparison of p, d, t, and ${}^3\text{He}$ spectra at 45, 60, 90, and 130 degrees from 800 MeV/nucleon ${}^{20}\text{Ne} + \text{NaF}$ measured at the Bevatron/Bevalac at the Lawrence Berkeley Laboratory [57, 58] with calculations by LAQGS03.03 using its “standard” version of the coalescence model ($p_0 = 0.09$ GeV/c for d, 0.108 GeV/c for t and ${}^3\text{He}$, and 0.115 GeV/c for ${}^4\text{He}$; dotted lines) and with modified values of p_0 labeled in legend as “coal1” ($p_0 = 0.15$ GeV/c for d, and 0.175 GeV/c for t, ${}^3\text{He}$, and ${}^4\text{He}$; dashed lines), as well as with a second modification of p_0 labeled in legend as “coal2” ($p_0 = 0.12$ GeV/c for d, and 0.14 GeV/c for t and ${}^3\text{He}$, and ${}^4\text{He}$; solid lines), as indicated (for simplicity, all calculations were done on a ${}^{20}\text{Ne}$ target).

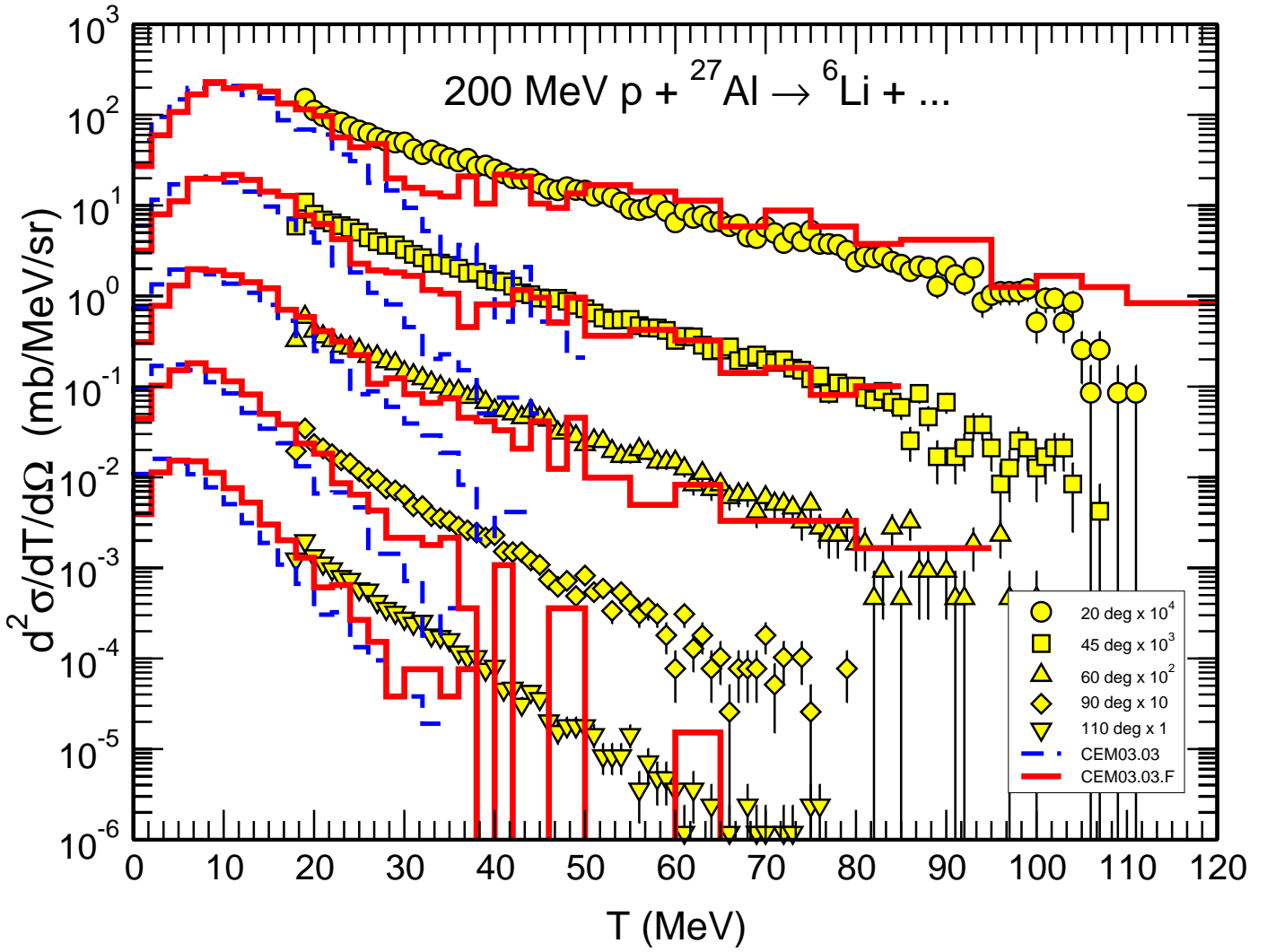


Figure 27: Comparison of experimental ${}^6\text{Li}$ spectra at 20, 45, 60, 90, and 110 degrees by Machner et al. [61] (symbols) with calculations by the unmodified CEM03.03 (dashed histograms) and preliminary results with the modified MEM in CEM03.03.F (solid histograms), as indicated.